(12)

Midterm Technical Report No. 4A *May 1976*
Covering the Period August 8, 1975 to April 15, 1976
SRI No. MP 76-46

NEW ELECTRONIC-TRANSITION LASER SYSTEMS

Part I: Electron Pumped Systems

By: M. V. McCUSKER, D. C. LORENTS, D. L. HUESTIS,
R. M. HILL, H. H. NAKANO, and J. A. MARGEVICIUS

Prepared for:

DEFENSE ADVANCED RESEARCH PROJECTS AGENCY
WASHINGTON, D. C. 20301
AND
U. S. ARMY MISSILE COMMAND
REDSTONE ARSENAL, ALABAMA 35809

ARPA Order No. 1180
Contract DAAH01-74-C-0524 (8 February 1974 to 15 August 1976)
Contract Amount $763,482

SRI Project PYU-3190

STANFORD RESEARCH INSTITUTE
Menlo Park, California 94025 · U.S.A.

Unclassified

SECURITY CLASSIFICATION OF THIS PAGE (When Data Entered)

REPORT DOCUMENTATION PAGE

READ INSTRUCTIONS BEFORE COMPLETING FORM

1. REPORT NUMBER

2. GOVT ACCESSION NO.

3. RECIPIENT'S CATALOG NUMBER

rept. no.

4. TITLE (and Subtitle)

New Electronic-Transition Laser Systems, Part I. Electron Pumped Systems.

5. TYPE OF REPORT & PERIOD COVERED

Midterm Technical 4A
8 August 1975 to 15 April 1976

6. PERFORMING ORG. REPORT NUMBER

SRI-MP-76-46

7. AUTHOR(s)

M. V. McCusker, D. J. Lorents, D. L. Huestis, R. M. Hill, H. H. Nakano, and J. A. Margevicius

8. CONTRACT OR GRANT NUMBER(s)

DAAH01-74-C-0524
ARPA Order-1180

9. PERFORMING ORGANIZATION NAME AND ADDRESS

Stanford Research Institute
333 Ravenswood Avenue
Menlo Park, California 94025

10. PROGRAM ELEMENT, PROJECT, TASK AREA & WORK UNIT NUMBERS

11. CONTROLLING OFFICE NAME AND ADDRESS

Defense Advanced Research Projects Agency
1400 Wilson Boulevard
Arlington, Virginia 22209

12. REPORT DATE

May 1976

13. NO. OF PAGES

67

14. MONITORING AGENCY NAME & ADDRESS (if diff. from Controlling Office)

U.S. Army Missile Command
Redstone Arsenal, Alabama 35809

15. SECURITY CLASS. (of this report)

Unclassified

15e. DECLASSIFICATION/DOWNGRADING SCHEDULE

16. DISTRIBUTION STATEMENT (of this report)

Distribution of this document is unlimited.

12 73p.

17. DISTRIBUTION STATEMENT (of the ebstract entered in Block 20, if different from report)

16 SRI-PYU-3190

intl on B doc.

18. SUPPLEMENTARY NOTES

19. KEY WORDS (Continue on reverse side if necessary end identify by block number)

excimer lasers, e-beam pumping, rare gas-halogen lasers

20. ABSTRACT (Continue on reverse side if necessery and identify by block number)

Considerable progress in understanding the kinetic processes involved in electron-pumped rare gas-halogen mixtures, particularly Ar/I_2, is reported. This gas system has great promise as a scalable, high-power laser medium capable of being pumped by electron beam, e-beam-sustained discharge, or nuclear fission fragments. The kinetic model involves the production of excited rare gas, followed by two very fast neutral energy transfer steps. The selective energy flow is simply represented as $Ar^* \rightarrow I^* \rightarrow I_2^*$ followed

DD FORM 1 JAN 73 1473

EDITION OF 1 NOV 65 IS OBSOLETE

SECURITY CLASSIFICATION OF THIS PAGE (When Data Entered)

332 500

20. Abstract (continuation)

by collisional relaxation of the $I_2^{(*)}$ to a single state radiating the 342.5 nm band with high fluorescence yield. We have made extensive experimental measurements testing this model and measuring the relevant rate coefficients and cross-sections. Kinetic steps involving halogen ions cannot be completely ruled out, but the results given here argue against their importance. Sustained discharge pumping is discussed briefly and a projected overall efficiency of approximately 20% is predicted.

CONTENTS

SUMMARY

We report progress in understanding the kinetic processes pertinent to rare gas molecular halogen lasers, particularly Ar/I_2. A tested kinetic model is vital to assess the potential of such media for efficient scalable high power lasers and to determine the rate constants and other essential data that are needed in the scale-up and optimization efforts.

In Section I we discuss the essential steps in the development of large scale, high energy lasers. In the context of energy transfer pumping of electronic transition laser media, the important microscopic processes and the roles they play in determining laser efficiency and scalability are identified. Having identified the key kinetic processes, the theoretical and experimental tools of atomic and molecular physics can be used to obtain rate coefficients, cross sections, and other parameters.

In Section II we introduce the basic model for energy transfer pumping of halogens from excited rare gases. The kinetics of excitation of the rare gases are reasonably well understood and provide the basis for the modelling of the energy transfer collisions with halogens. In Ar/RI mixtures a two-step energy transfer model is proposed involving an intermediate dissociative process that produces I^* which subsequently reacts with the halogen containing additive to produce an ionic state of I_2. This ionic excited state of I_2, which radiates at 342.5 nm, very effectively, concentrates the energy flow from the intermediate atomic states and thereby provides the mechanism for the observed high fluorescence yield.

A detailed report of the experimental measurements carried out on various rare gas/halogen additive mixtures is given in Section III. Short pulse e-beam excitation of the gases is used to produce the radiation whose intensity and spectral composition is determined. The temporal

behavior of the emissions are followed and their dependence on gas composition and density are used to obtain formation and decay rates. The radiative lifetime of the I_2^* upper level was determined as well as the relevant energy transfer rate coefficients.

Finally, the current status of the Ar/I_2 kinetic model is evaluated in terms of the experimental observations and other information available from the literature. It is concluded that this medium shows excellent prospects for an efficient, scalable laser at 342.5 nm. It appears that the medium is suitable for pumping by e-beams, e-beam sustained discharges, or neutron generated fission fragments.

TABLES

ILLUSTRATIONS

I MICROSCOPIC PROCESSES IN THE DEVELOPMENT OF EFFICIENT HIGH ENERGY LASERS

A. Introduction

The development of efficient high energy lasers operating at visible or near ultraviolet wavelengths, under DARPA support, has progressed extremely rapidly in the last few years. Based largely on the concept of energy transfer from excited rare gases to specific excited states of acceptor molecules, several lasers have reached the demonstration stage and show promise of efficient operation at high power levels. In the near future, difficult decisions must be faced in choosing and optimizing laser systems for scale-up. Among the decisions to be made are:

1. The choice of laser medium
2. The choice of pumping scheme
3. The choice of operating conditions

Figure 1 illustrates the stages in laser development. Once a candidate has been identified and demonstrated, the laser medium must be well characterized with respect to efficiency, scaling, and operating parameters before a large scale-up is undertaken. The medium characterization is difficult, requiring detailed understanding of the energy deposition kinetics, the energy transfer kinetics, and the coupling of the radiation field to the medium. Small-scale laser demonstration is clearly inadequate for characterizing a medium for scale-up, where the operational parameters vary widely from those of the demonstration laser.

The success of a laser device development program requires the fullest use of the talents of the investigators. In particular, neither a purely empirical nor a purely analytical approach alone is likely to succeed. The successful development of a device requires a detailed understanding of the microscopic processes that define the physically

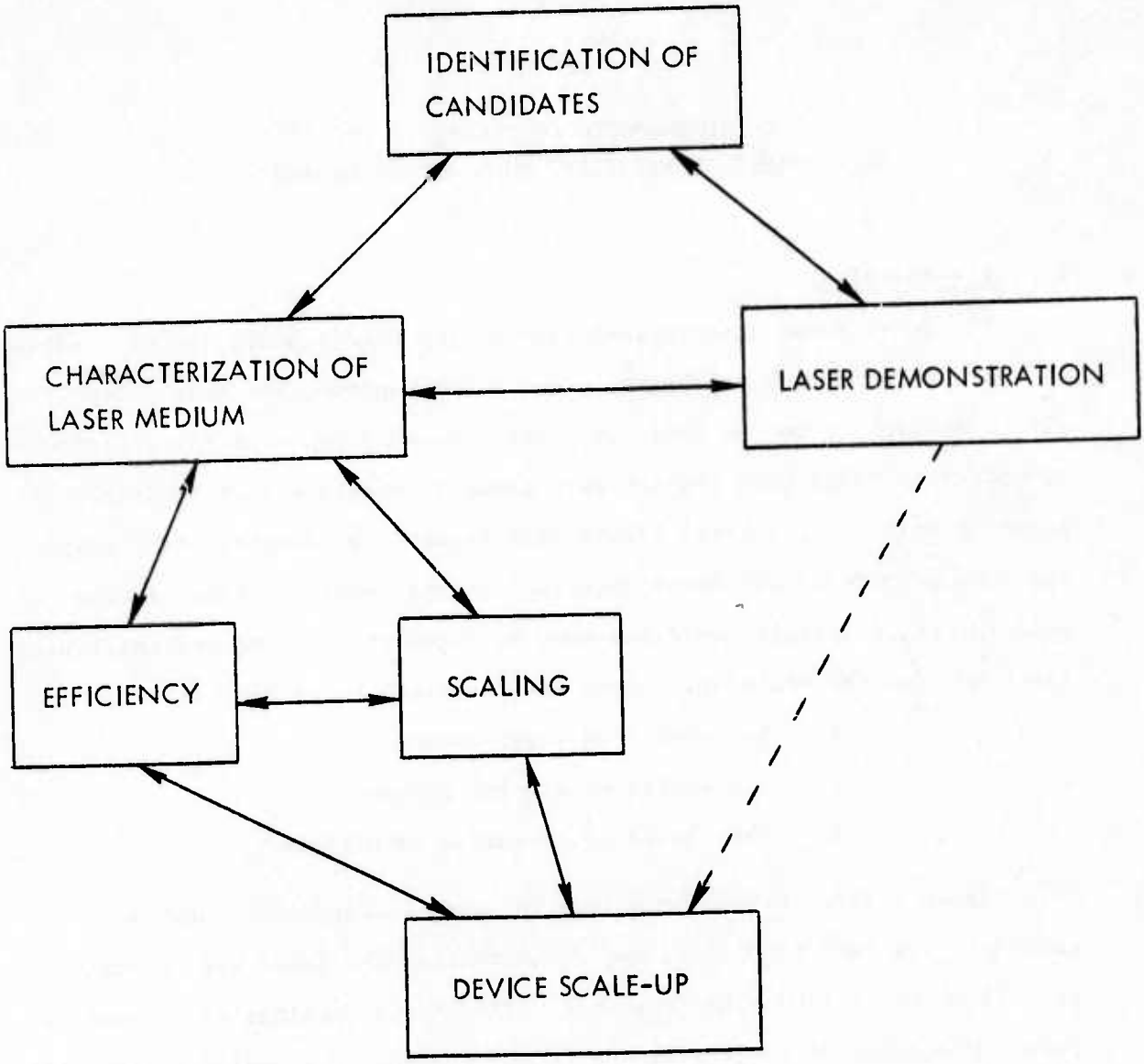

Figure 1. Stages of Laser Development

available options. Some of these microscopic processes and their impact on laser development are described below.

B. Efficiency

A number of promising candidate systems have been identified to date. Several of these have demonstrated laser action, and a few appear to have efficient energy output. Optimization of these candidates depends on improved efficiency and scaling to higher output energies. Table I illustrates some of the factors entering into the efficiency analysis of candidate systems. All schemes for converting stored electrical, chemical, or nuclear energy into laser output require a sequence of energy transfer steps, each of which must be efficient to produce an efficient laser. Some of the problems inherent in any candidate laser medium and pumping scheme can be circumvented, but others restrict the choice of a candidate system despite the preliminary indications. Some of these problems are now described.

1. Deposition

The development of electron-beam pumped electronic transition lasers has been motivated largely by a rather complete understanding of the processes of energy deposition in rare gases [LO72,LEH73]. An efficiency approaching 50% can essentially be guaranteed under the proper conditions for the production of rare gas-excited states [L76]. This deposition efficiency is applicable to neutron/fission-fragment pumping in which the dominant deposition mechanism is also ionization by secondary electrons [LMR76]. Discharges and electron-beam sustained discharges are potentially considerably more efficient in their energy deposition. However, in the discharge case, the efficiency depends strongly on the details of the electron distribution function and its dependence on the energy variation of the excitation and loss cross sections. Several specific loss processes have been identified, such

Table I

EFFICIENCY FACTORS

1.	Primary Pump	Electron-beam pulse forming and foil losses
		Neutron production
		Capacitor energy coupling
		Chemical energy storage
2.	Deposition	Neutron-fission cross sections
		W-value for electrons and fission fragments
		Electron excitation and loss cross sections
		Preparation and mixing of reactants
3.	Energy	Energy transfer and reaction branching ratios
		Quenching reactions
4.	Quantum	Ratio of output photon to energy of pumped level
5.	Extraction	Stimulated emission cross section
		Absorption losses
		Bottlenecking
		Photon-kinetics interactions

as electron excitation of the lowest laser level, electron impact mixing, excitation and ionization of excited states, and vibrational excitation of additive molecules. An understanding of these processes is essential when choosing gas mixture, pumping rate, and electron energy distribution in the development of large discharge pumped lasers.

2. Energy Flow

Once the energy is deposited in the gas, it must be selectively channeled into the desired upper laser level. Each energy transfer, association, or chemical reaction must be energetically or mechanistically restricted to the desired path. Particularly effective in channeling electronic excitation energy to a single level are the strongly ionic states formed by harpooning reactions, for example, in the rare gas halides and rare gas halogens.

$$Kr^* + F_2 \rightarrow KrF^* + F$$

$$I^* + HI \rightarrow I_2^* + H$$

Quenching reactions can interfere in two basic ways. First, quenching of the upper laser level lowers the efficiency and gain. However, these factors need not be degraded if bottlenecking can be avoided (as described below). Second, quenching may divert an energy transfer precursor. For example, Kr^* may, by three-body association, form Kr_2^*, which radiates instead of following the desired energy transfer path.

3. Extraction

A bright fluorescence does not imply gain, nor population inversion. Further, the existence of lasing in a medium does not ensure that radiative energy can be efficiently extracted. The laser medium may have losses caused by absorption of the unexcited gas and various transient species of the excited gas. Further, the upper level itself may have a greater cross section for absorption than for stimulated

emission. This has been found to be a problem for the rare gas [LEH73] and mercury excimers [HEL73].

Even if the lower laser level is not pumped directly, it will fill rapidly through radiative transitions from the upper laser level. Bottlenecking will occur if the lower level is not preferentially quenched. This is always true, even when an intense laser field is present. The output power is limited both by the rate of pumping and by the rate at which the lower level is emptied. This limitation has motivated the use of excimer laser molecules in which dissociative lower level empties during the period of a single vibration. An increase in the laser photon flux can then overcome the potential quenching of the upper laser level. This principle is used to advantage in the KrF laser. The XeF laser may have more critical operating conditions because of its bound lower level. In that case, raising the gas temperature and lowering the xenon pressure may decrease the equilibrium concentration of ground state XeF.

Finally, the presence of an intense optical flux at short wavelengths could interfere with the energy flow kinetics. Several of the important reaction intermediates could absorb the laser photons. Because of their low concentration, this may not affect the gain, but photodestruction of the reaction intermediates may interfere with the kinetics and limit the obtainable fluxes.

Table II illustrates some important limitations to the optical fluxes necessary to overcome quenching but avoid bottlenecking, instabilities and other high flux problems. These inequalities aid in the selection of candidate systems and their operating conditions if the appropriate rate constants an cross sections are known.

C. Scaling

The development of large devices requires the consideration of several factors listed in Table III. Some of the possible difficulties

Table II

SOME PHOTON FLUX INEQUALITIES

○ AVOID QUENCHING $I_2^* + I_2 \rightarrow$ Quenched k_q vs $I_2^* + h\nu \rightarrow I_2^{\ddagger} + 2h\nu$ σ_{se} Conclude $\Phi \gg \frac{k_q I_2}{\sigma_{se}}$	● AVOID BOTTLENECKING $XeF^{\ddagger} + M \rightarrow Xe + F + M$ k_ℓ vs $XeF^{\ddagger} + h\nu \rightarrow XeF^*$ σ_{se} Conclude $\Phi \ll \frac{k_\ell M}{\sigma_{se}}$
● AVOID DISTURBING KINETICS $Kr^* + F_2 \rightarrow KrF^* + F$ k_r vs $Kr^* + h\nu \rightarrow Kr^+ + e$ σ_{PI} Conclude $\Phi \ll \frac{k_r F_2}{\sigma_{PI}}$	○ AVOID INSTABILITIES $e + F_2 \rightarrow F + F^-$ k_a vs $F^- + h\nu \rightarrow F + e$ σ_{PD} Conclude $\Phi \ll \frac{k_a F_2}{\sigma_{PD}}$

Table III

SCALING FACTORS

- Power Density
- Active Volume-Length
- Pumping Time

SCALING REQUIREMENTS

- Scalable Primary Pump and Deposition
- Only Linear Losses
  - No excited state-excited state losses
  - No electron-excited state losses
  - No photon-excited state losses
- Stability
  - No parasitic oscillation
  - No photon induced instabilities
- Homogeneity
- Waste Heat Dissipation

are already being studied. Others are potentially very serious and must be better understood before large devices can be constructed.

1. Scalable Pumping

The size and cost of current electron beam machines discourage scale-up. Electron-beam driven lasers are limited in size by distance of electron penetration and in pumping rate by self-fields [HO76]. In terms of scalability and uniformity of large volume pumping, neutron/fission-fragment pumping offers considerable advantages, while retaining favorable kinetics. Discharges and electron-beam sustained discharges are potentially scalable to large volumes, but scale-up will impose severe requirements for electrical stability and for selective energy flow kinetics.

2. Nonlinear Losses

Because of the required high pumping rates, interactions of the excited states with each other, with electrons, and with the photon field must be considered. Excimer-excimer collisions were quickly recognized as a limiting factor in the rare gas lasers [LO72]. Electron-excited state collisions have also been recognized as important loss processes in high power electronic transition lasers and appear to be a limiting factor in any discharge-pumped, rare gas dominated laser medium. Photoabsorption by the excited states, not necessarily the upper laser level, is another loss factor. Any of these losses that rises faster than linearly with power can limit laser scalability.

3. Stability

Storage of large amounts of energy per unit volume may cause unstable operation. Some of the nonlinear losses referred to above may cause the stored energy to be released, for example, by parasitic oscillation along the transverse laser dimensions or arcing through a rapidly growing electron density. As laser scaling progresses, instabilities arising from unexpected absorption of the laser flux will be of increasing concern.

4. Homogeneity

Homogeneity, a requirement for high optical quality, may be difficult to obtain. Uniform pumping is required. The refractive indices of high pressure gases at short wavelengths may require operation at lower pressures or extremely high energy pulses with low repetition rates to allow for gas replacement.

5. Waste Heat Dissipation

Gas heating can have either detrimental or beneficial effects on laser operation. Thermal population of the lower laser level could become serious. Dissociation of the reactant molecules may limit the laser pulse energy or repetition rate.

D. Conclusion

Several aspects of high-energy laser-media must be understood to guide decisions on the development phase of the program. The list of potentially scalable candidate systems is not large. We know relatively little about the details of the laser medium; for example, how to select the optimum pump-medium combinations, or how the medium will respond to the intense optical laser flux. As the development program progresses, the areas of difficulty will become more apparent. A more complete understanding of the laser medium is essential to

(1) Guide the selection of efficient, scalable candidates

(2) Recommend optimal operating conditions

(3) Allow more rapid interpretation of the results of optimization attempts

(4) Provide possible redirection toward more effective approaches.

The kinetic complexity of the lasing medium itself prevents it from being an optimal environment for isolating the dominant microscopic processes and measuring their rates. Many of these processes may be identified in advance. The laser medium can then be rapidly characterized, with special emphasis on efficiency and scaling, based on careful experimental and analytical study of important known microscopic processes.

II INTRODUCTION TO THE RARE GAS/HALOGENS

A considerable effort is under way in the development of high energy lasers based on electron pumped mixtures of rare gases with halogen-containing molecules. Many such lasers have now been demonstrated: XeBr [SH75], XeCl [EB75a], XeF[BE75,ABB75], KrCl [MP76], KrF [EB75a, BBA76,THH75], Ar/I_2 [EB75b,BAB75,HHT75], Ar/Br_2 [MST76]. For each of these lasers, the high pumping rates available from electron-beam excitation were used in the initial demonstration. The concept that these laser media may be efficiently and scalably pumped at high repetition rates with a discharge is extremely attractive. The possibility of nuclear pumping also needs to be examined carefully. The transition from one pumping scheme to another requires a thorough assessment of the various efficiency and scalability factors, and therefore, a thorough characterization of the laser medium itself.

First, it is essential to understand the energy flow kinetics. These kinetics are complicated, involving a sequence of kinetic steps. In particular, the measurable quantities (fluorescence intensity, decay time, laser output, and the like are not trivial functions of the gas mixture, pumping conditions, and output coupling. A list, as short as possible, of the critical processes must be established and used to characterize the response of the laser medium. The values of the critical rates and cross sections must then be determined.

Our ongoing study of the electron-beam rare gas/halogen and rare gas halide systems begins with the well known rare gas deposition kinetics [WGH74,LEH73]. Next, we postulate a physically reasonable mechanism for the energy flow from the rare gas through the halogen-containing additive to the upper laser level. We include only those reactions necessary to explain the experimental results and use the experiment to determine their

rates. This operational procedure for developing and refining a kinetic model has been extensively illustrated in our previous reports [HGH74, HGH75, GHH75].

We will now discuss our studies of rare gas/halogen systems, in which we use a very short burst of high energy electrons to excite the gas mixture. Under most conditions, the excitation pulse is short compared with the subsequent chain of energy transfer reactions, and kinetic rates can be obtained from the temporal behavior of the optical emissions. Once the kinetic reaction mechanisms and the rates of individual reactions are known, they can be applied to other pumping methods. such as discharge or nuclear.

The basic block diagrams for the Ar/I_2 reaction chain is shown in Figure 2. The specific reactions involving the initial rare gas excitation have been studied for the excimer laser, and models have been developed by George et al. [LEH73]. The most relevant reactions are listed in Table IV. In the pressure range of interest, 0.5-10 atm, the excitation and the redistribution of the energy into the argon metastable states is very fast compared with most of the other reactions. Indeed, the argon kinetics can be summarized: electron-beam deposition produces an almost instantaneous source of Ar^*, which may form argon excimers (Ar_2^*) through Reaction (3) (Table IV) or react with and transfer energy to an additive molecule as in Reaction (8). The argon excimers may participate in subsequent energy transfer reactions, or may radiate 126 nm photons.

In homonuclear halogen lasers, this energy is transferred by collisions with the additive vapor to form excited neutral halogen atoms (I^*). In a subsequent collision, this energy is transferred through a reactive collision to the molecular additive to form excited molecular halogen (I_2^*). This excited state is ionic in character and can radiate rapidly to a lower covalent excited state.

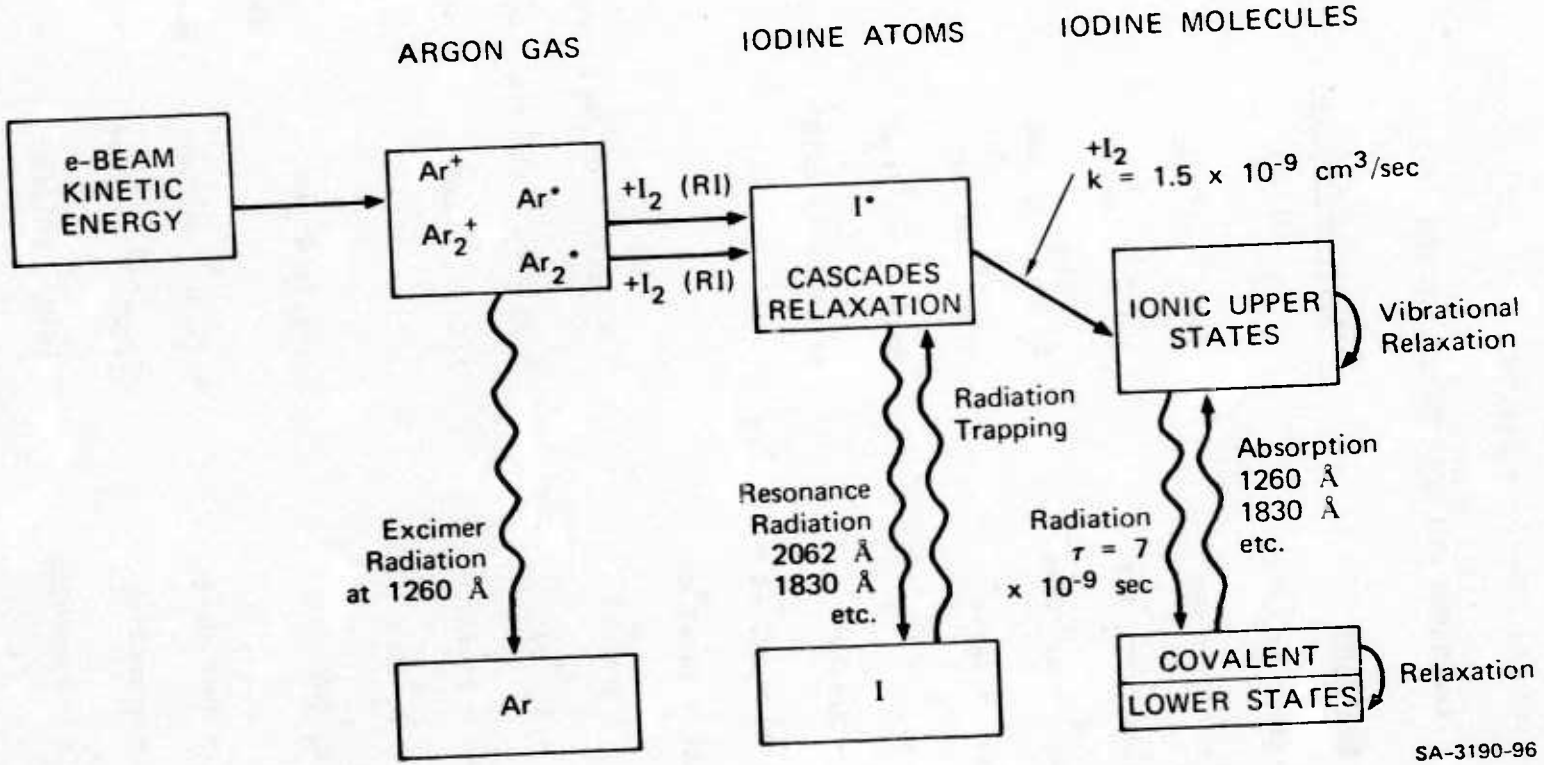

Figure 2. Energy flow diagram for Ar/I_2 kinetic model.

Table IV

REACTIONS AND RATE CONSTANTS FOR Ar/I_2

	Reaction	Rate Coefficient	Reference
(1)	$Ar^+ + 2Ar \rightarrow Ar_2^+ + Ar$	2.5×10^{-31} cm^6/sec	L76
(2)	$Ar_2^+ + e^- \rightarrow Ar^* + Ar$	1×10^{-6} cm^3/sec	"
(3)	$Ar^* + 2Ar \rightarrow Ar_2^* + Ar$	1×10^{-32} cm^6/sec	"
(4)	$Ar^* + Ar^* \rightarrow Ar^+ + Ar + e^-$	5×10^{-10} cm^3/sec	"
(5)	$Ar_2^* + e^- \rightarrow 2Ar + e^-$	1×10^{-9} cm^3/sec	"
(6)	$Ar_2^* + Ar_2^* \rightarrow Ar_2^+ + 2Ar + e^-$	5×10^{-10} cm^3/sec	"
(7)	$Ar_2^* \rightarrow 2Ar + h\nu$	variable to 4×10^7	"
(8a)	$Ar^* + RI \rightarrow ArI^* + R \rightarrow Ar + I^* + R$		
(8b)	$Ar_2^* + RI \rightarrow 2Ar + I^* + R$		
(8c)	$Ar^* + I_2 \rightarrow Ar + I^* + I$	$1.8\pm.2\times10^{-9}$ cm^3/sec	measured
(9a)	$I^* + I_2 \rightarrow I_2^{*+} + I$	$1.3\pm.2\times10^{-9}$ cm^3/sec	measured
(9b)	$I_2^{*+} + Ar \rightarrow I_2^* + Ar$	$7\pm3\times10^{-11}$ cm^3/sec	"
(9c)	$I^* + RI \rightarrow I_2^* + R$		
(10)	$I_2^* \rightarrow I_2^{\ddagger} + h\nu$	$1.4\pm.2\times10^8/sec$	measured SMC76
(11a)	$I_2^* + I_2 \rightarrow$ quenching	$\leq 1\times10^{-9}$ cm^3/sec	measured
(11b)	$I_2^* + HI \rightarrow$ quenching	$4\pm2\times10^{-10}$ cm^3/sec	"
(11c)	$I_2^* + CF_3I \rightarrow$ quenching	$\leq 1\times10^{-9}$ cm^3/sec	"
(12)	$I^+ + I^- + Ar \rightarrow I_2^* + Ar$	see text	JKB65
(13)	$e + I_2 \rightarrow I^- + I$	$1\text{-}4\times10^{-10}$ cm^3/sec	T69

Table IV (Continued)

	Reaction	Rate Coefficient	Reference
(14)	$h\nu(120\text{-}180nm)+RI \rightarrow I^{*}+R$	$\sigma \cong 10^{-16}$ cm^2	MS70
(15a)	$Ar^{*}+RI \rightarrow RI^{+}+e$		
(15b)	$Ar_2^{*}+RI \rightarrow RI^{+}+e$		
(15c)	$h\nu(126nm)+RI \rightarrow RI^{+} + e$		MHI60
(16)	$RI^{+}+e \rightarrow I^{*}+R$	10^{-6}-10^{-7}	estimate
(17)	$I_2^{*}+h\nu(342.5nm) \rightarrow I_2^{\ddagger}+2h\nu$	$\sigma_{se} = 1.3\pm0.2\times10^{-15}$ cm^2	calculated for bandwidth of 2 nm for B state
(18)	$I_2^{\ddagger}+Ar \rightarrow I_2+Ar$	$\sim 2\times10^{-11}$	CB73
(19)	$I^{-}+h\nu(342$ nm)	$2\pm1\times10^{-17}$ cm^2	R69
(20)	$I^{*}+h\nu \rightarrow I^{+}+e$	$\sigma \leq 10^{-17}$ cm^2	estimate from hydrogenic theory

The above, rather general, scenario applies to argon/bromine mixtures and argon/chlorine mixtures except that in the latter case, both Cl_2^* and $ArCl^*$ are observed. However, the dominant emission from argon/fluorine mixtures is from ArF^*, and we have not yet observed F_2^*. The additive vapor need not be homonuclear; it can include a limited selection of additives, RX, such as HI, CH_3I, CF_3I, HBr, HCl, etc. The observed fluorescence is emitted by the homonuclear halogen. The energy levels relevant to the noble gases, the homonuclear halogens, and the hydrogen halides are summarized in Figure 3.

Setser's suggestion that rare gas atoms in their lowest Rydberg states resemble alkalies in their reactions with halogen molecules provides insight into the selectivity of the energy flow scheme in the reaction of Ar^* + RX [GT74, RS75]. The reaction mechanism is the well known "harpoon reaction" (also referred to as the charge transfer reaction) in which strongly bound ionic states with long range interactions are populated by curve crossings with initial covalent states. This mechanism explains the efficient channeling of energy from various initial excited states to the radiative state. This reaction mechanism plays the dominant role in the energy flow in all the rare gas/halide and rare gas-halogen systems. A recent review [GSC76] discusses these reaction mechanisms in more detail. In some cases, the reaction proceeds in a single step to the lowest ionic level from which it radiates, e.g.,

$$Ar^* + F_2 \rightarrow ArF^* + F$$

while in other cases, two or more steps are required, such as in Ar/I_2

$$Ar^* + I_2 \rightarrow ArI^* + I \rightarrow Ar + I^* + I \qquad (8c)$$

$$I^* + I_2 \rightarrow I_2^* + I \qquad (9a,b)$$

In both cases, the initial step involves the formation of a rare gas halide, which either is bound or predissociates, depending on the energy levels

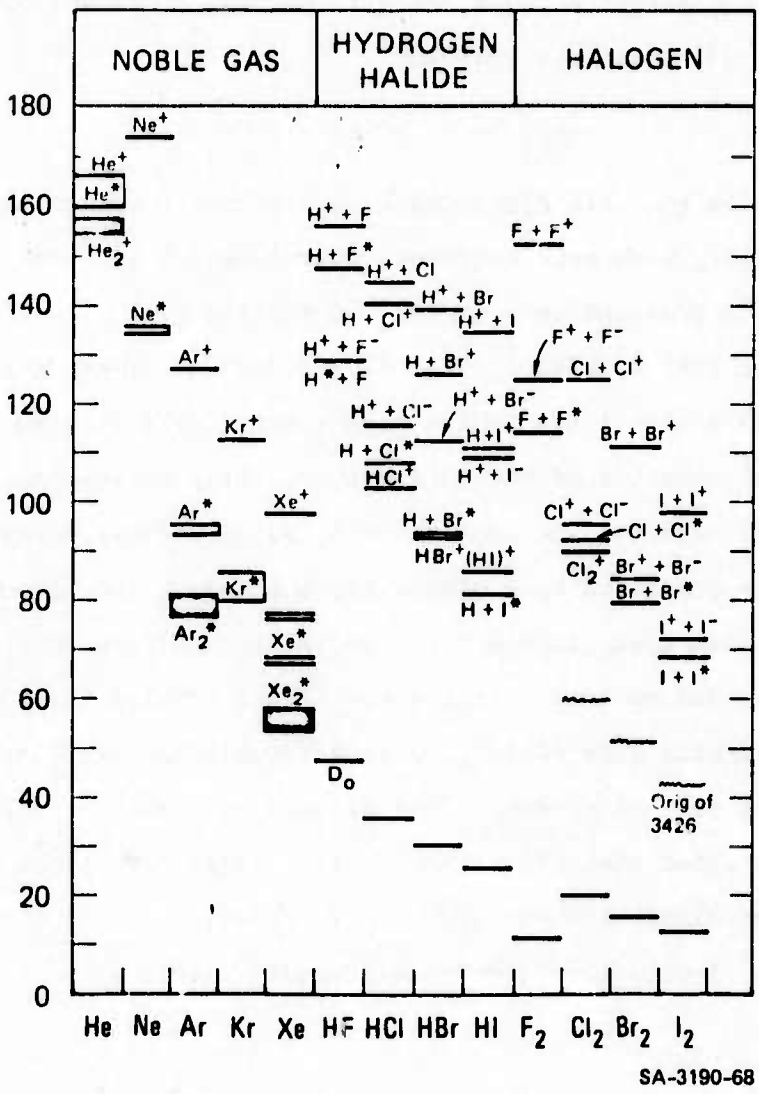

Figure 3. Halogram. Energy levels for Ar/Halogen/ Halide System. Ordinate is in cm^{-1}. Lowest molecular level is the dissociation limit.

of the reactants. The Ar/Cl_2 system is an intermediate case in which both $ArCl^*$ and Cl_2^* are observed to radiate. In the case of I_2 and Br_2, the intermediate atomic I^* or Br^* has been confirmed experimentally in both our work and that of Setser et al. [GSC76].

In the simplest picture, excited halogen atoms are produced both by the collisional reactions (8a) and

$$Ar_2^* + I_2 \rightarrow 2Ar + I^* + I \quad . \tag{8b}$$

Based on the work discussed here, we conclude that these reactions are very rapid, with rate constants near $1.8\pm.2 \times 10^{-9}$ cm^3/sec. The excited iodine may be produced in a variety of excited states. We have observed radiation at 2067 Å, 1783 Å, 1830 Å, and 1673 Å. These transitions are indicated on a simplified iodine atom energy level diagram (Fig. 4). The temporal behavior of the intensity of these emissions indicates the same general behavior, in particularly, similar decay rates, each of which can be described by a single exponential. Since ground state fine structure relaxation rates and the recombination rate for the formation of molecular iodine from iodine atoms should be slow relative to the important kinetic time scales, we expect radiation trapping effects to be important for the atomic iodine radiations. This extends the effective excited state lifetimes substantially and allows energy transfer reactions of I^* to proceed effectively.

The I^* energy transfers to the additive vapor:

$$I^* + I_2 \rightarrow I_2^* + I \quad , \tag{9a,b}$$

$$I^* + RI \rightarrow I_2^* + R \quad . \tag{9c}$$

We have measured the rate constant of the first reaction to be $1.3\pm0.2 \times 10^{-9}$ cm^3/sec. The molecules produced by this reaction subsequently collisionally relax and radiate in the 343 nm band. The spectroscopic details are discussed in Section III. We have measured the radiative lifetime

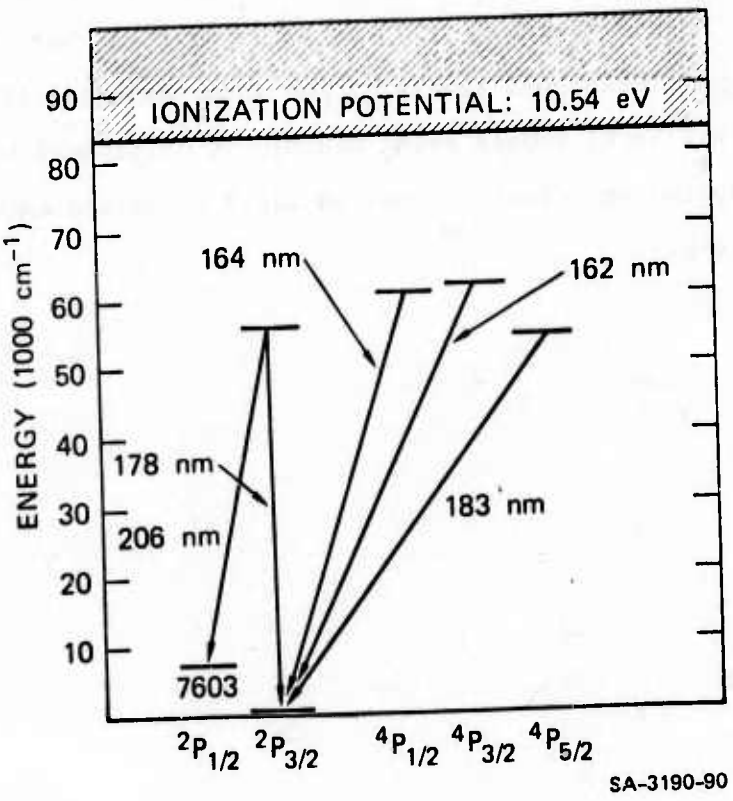

Figure 4. Energy level diagram of I atom showing the first few excited states and the wavelengths emitted.

of this upper state to be 7 ± 1 ns. The above reaction may produce a variety of electronic and vibrational states. However, before radiation, these states are rapidly converted to a single manifold whose spectroscopic details have been thoroughly discussed by several authors [see M71].

Whatever the spectroscopic assignments for the upper and lower states of the 343 nm band, it is generally agreed that the transitions lead to high vibrational levels of the lower state as illustrated in Fig. 5. This level should relax rapidly by collisions with noble gas atoms, reducing any complications in laser operation caused by bottlenecking.

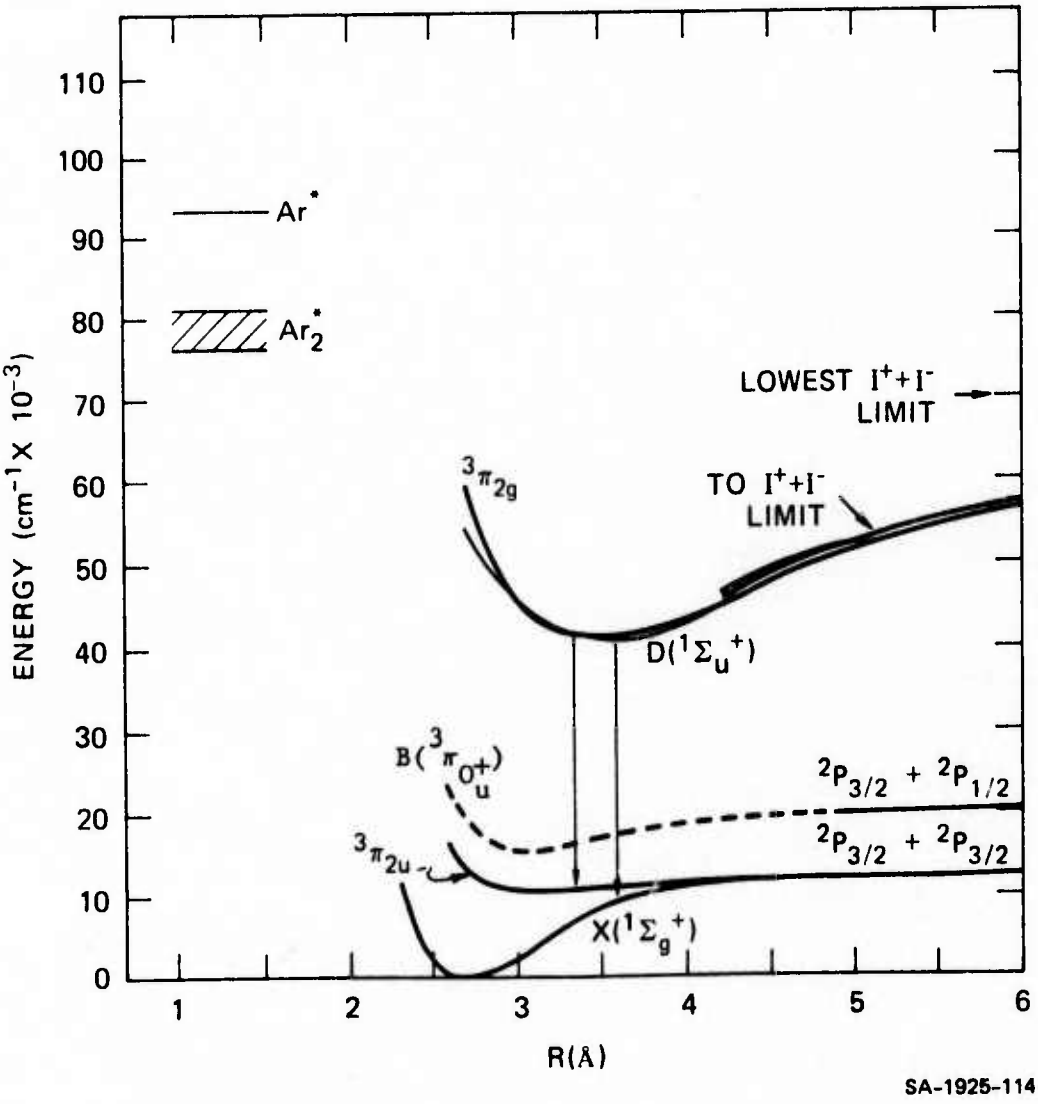

Figure 5. Energy levels for Ar/I_2 energy transfer. Many of the possible I_2 levels are not shown. See [M71] for more detail.

III THE EXPERIMENTAL PROGRAM: TECHNIQUE AND DATA

A. Experimental Apparatus and Procedure

The experimental apparatus is quite similar to that described in our previous reports [HGH75], and is shown schematically in Figure 6. Optical emissions, resulting from the pulsed electron excitation of a gas mixture under high pressure, are viewed by a 0.5 meter monochromator-spectrograph (McPherson model 216.5). A Febetron 706 (Hewlett Packard) provides a 2 to 3 nsec, 6000 A pulse of 600 keV electrons, which enter the stainless steel experimental cell through a 1-mil-thick Inconel foil. By evacuating both the spectrometer and the tube between the cell window and the spectrometer entrance slits, we have obtained vacuum uv measurements down to the Ar_2^* excimer wavelength of 1260 Å. The cell windows are made from MgF_2.

The stainless steel cell has a central body containing a cavity 2.5 cm in diameter by 25 cm long; the electron beam is incident on the center of this cylinder so that the light path travels through $\simeq$ 12.5 cm of gas mixtures. The cell is designed to operate with sample gas pressures between 0 and 10,000 torr (approximately 0 to 15 atm). The 1-mil-thick Inconel foil window through which the electron beam enters is mounted so that the volume viewed by the spectrometer includes the foil surface. A rotating vane driven by magnetic coupling is used to mix the gases.

In handling the homonuclear halogens, reactions of the additive vapor with the cell walls must be avoided. We coated the interior of our cell with carbon (from an Aquadag suspension). A variety of other coating materials may be used, for example, a Teflon coating. Also, a particularly simple solution would be to construct the cell entirely from monel.

We established the iodine vapor pressure in the cell by adjusting the temperature between -20°C and + 80°C. The temperature was set by flowing an appropriate temperature bath solution (dry ice/acetone or heated water)

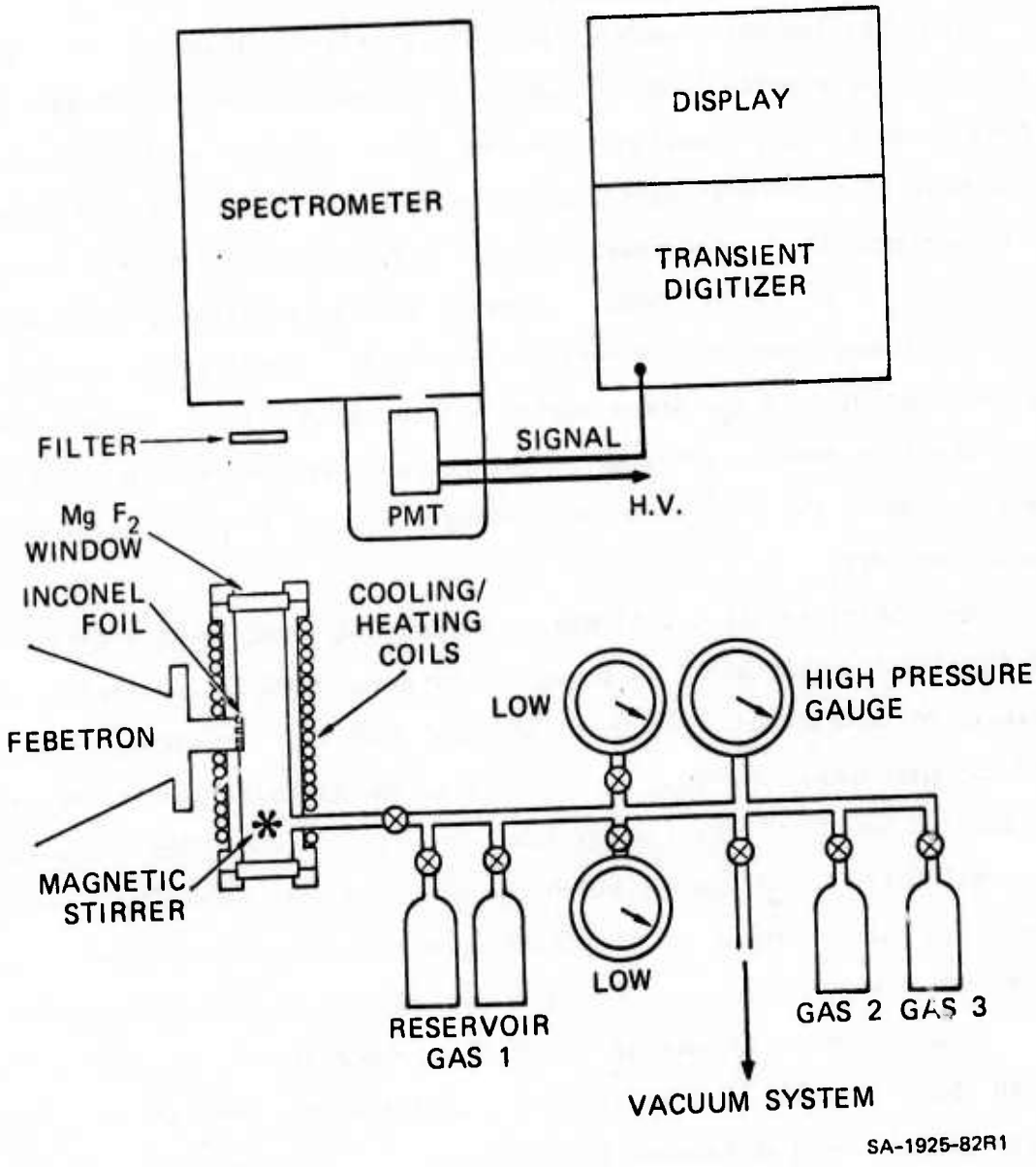

Figure 6. Block diagram of apparatus.

through a series of 1/4-inch copper coils wrapped around the cell. The vapor pressure was taken from the values published by Nesmeyanov [N63]. We checked the linearity of this method by making optical absorption measurements at various wavelengths and found it satisfactory.

The vapor pressure of the halogen-bearing gases (CF_3I, HI, CH_3I, as well as Br_2, HBr, Cl_2, and HCl) was set by a dilution technique. The gas was admitted to the empty cell to a pressure readable by a Bourdon gauge (several torr), and argon was added to bring the total pressure up to several atmospheres. The pressure of the mixture was reduced by pumping, and additional argon added to obtain the proper partial pressure of halogen gas.

For most of the work reported here, time-resolved measurements were made by recording the electronic signals from a fast phototube (generally a 1P28, coated, if necessary, with sodium salicylate for vacuum-uv measurements) with Polaroid photographs of an oscilloscope trace (Tektronix 485). Some of the data were recorded with a Tektronix WP2222 waveform processing system. With this system, we could "signal average" repeated events to reduce noise fluctuations in the signal. This was particularly useful in recording very fast events near the signal leading edge, and in measuring weak signals at very late times. Before averaging, we verified that the signal being observed was not subject to systematic intensity or decay time variation with Febetron shot number. With the waveform processing systems, decay times were determined by a least squares fit to the logarithm of the data points in the late time portion of the emission.

To make measurements of integrated intensity, we integrated the time-resolved signal recordings over time, and then repeated these measurements over all wavelengths to obtain a wavelength integration. This method eliminates problems of film nonlinearities.

We also made spectrometric studies of the emission from Ar/I_2 mixtures by exciting the gas with the modulated beam of a 200 keV, 100 μA electron accelerator. Data were recorded on an X-Y plotter from the output of a lock-in amplifier connected to the phototube.

We have used the previously published results [HGH74] from the kinetic modeling of Ar/N_2 mixtures to provide a convenient intermediate intensity standard. At several different points during this work, we removed the Ar/I_2 (or other mix) from the cell and directly substituted a mixture of Ar plus 5% N_2. By observing the N_2 2+ emission (at, for example, 357.6 nm) we could make rapid comparisons. This method eliminates accounting for geometrical factors associated with different sources, since it is the intensity ratio that is significant.

During these measurements, we recalibrated our spectrometer/detector system and included the use of a 1P28 phototube coated with sodium salicylate.

B. Halogen Spectra and Identification

Figures 7, 8, and 9, respectively, show the emission spectra of I_2, Br_2, and Cl_2 excited by energy transfer from Ar. Except for relative intensity, these spectra appear to be essentially independent of the original source of the halogen. We have used I_2, CH_3I, HI and CF_3I, Br_2 and HBr, as well as Cl_2 and HCl.* All these spectra show a complex behavior in the region of the major peak and a long series of red degraded bands with intensities decreasing toward shorter wavelengths. These bands have been previously observed in emission when the halogen is excited by absorption or electrical discharge in the presence of a foreign gas. Several observers have attempted to assign these bands,

---

With iodine we have used He, Ar, and Kr as the host gas with no essential alterations in the spectrum. When small amounts of xenon are added to the Ar/I_2 mixtures, XeI emission is observed in addition to the I_2 343 nm band.

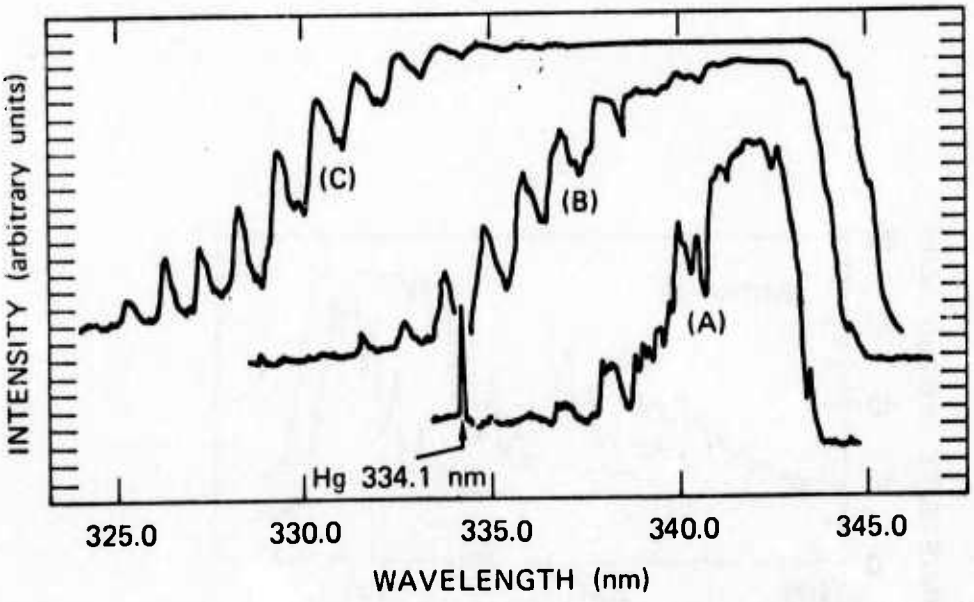

NOTE: Due to film saturation effects the vertical sceles are not linear end these data ere presented for illustrative purposes only. Curve A is for two Febetron shots, Curve B is for 5, end Curve C is for 30. Also in the diegram is e single line from a mercury calibretion source which is shown to illustrete the spectrometer resolution. These spectre were teken in second order.

SA-1925-115

Figure 7. I_2 emissions in Ar/I_2 mixture (2 atm Ar/ 3 torr I_2)

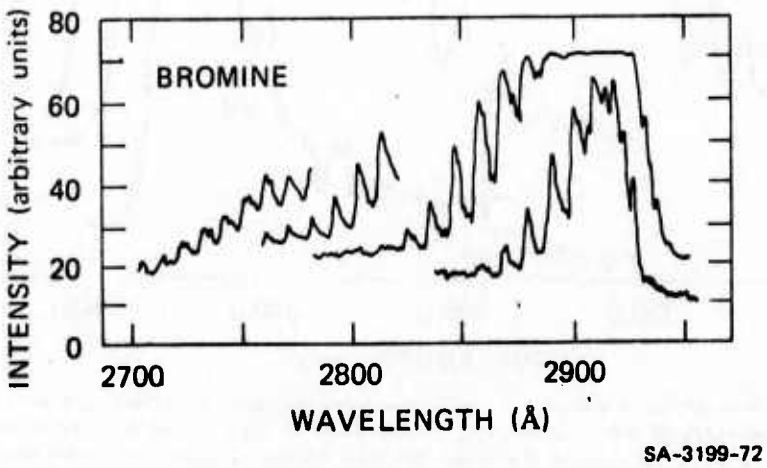

Figure 8. Spectra of Br_2 emissions in Ar/Br_2 mixture. However, wavelength traces are for higher excitations. Saturated portions of the spectra are omitted.

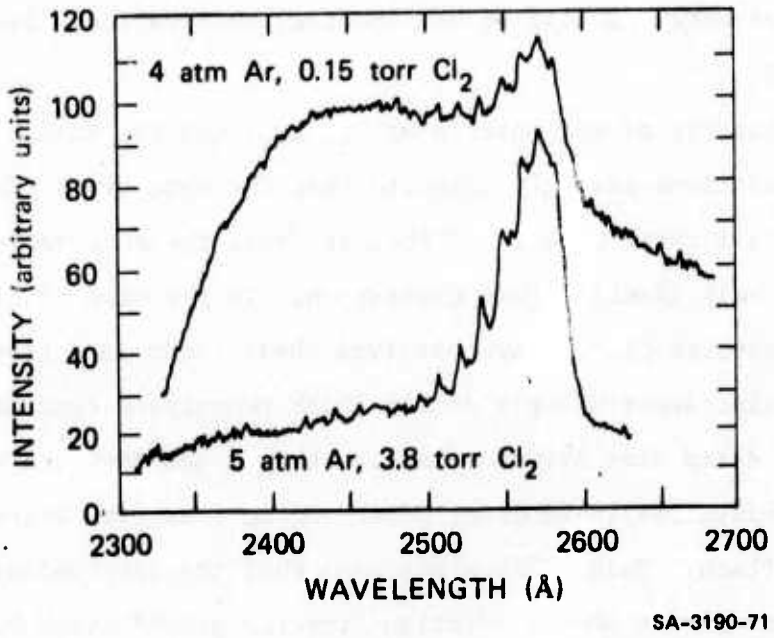

Figure 9. Spectra observed in Ar/Cl_2 mixtures.

but no concensus has yet been reached on this problem. In the case of I_2, Mulliken [M71] has given an excellent summary of the various interpretations of the 3425 Å bands as of 1971. He concludes that it is not possible to decide between Verma's [V58] assignments as 1432 $^3\Pi_{0_g^+} \rightarrow B\,^3\Pi_{0_u^+}$ and Tellinghuisen's [M71,WTN72] assignment as 1432 $^3\Pi_{2g} \longrightarrow {}^3\Pi_{2u}$ transition More than one upper state may be involved, because these emissions appear only in the presence of a foreign gas perturber that may collisionally mix the original excited level with the radiating level. This suggestion is supported by the pressure dependence of the radiative lifetime observed in our experiments, as well as the spectral observations discussed by Mulliken [M71].

The similarity of the spectra of I_2, Br_2, and Cl_2 excited under high pressure conditions strongly suggests that the same transition is being observed in all three cases. If that is true, the observations in Cl_2 and Br_2 can help identify that transition. In the case of Cl_2 and Br_2, Briggs and Norrish [BN63] have observed these bands in a transient absorption experiment using a double flash photolysis apparatus. By varying the delay time between flashes, they found that the transient absorption maximizes 10-20 μsec, depending on pressure, after the initial photolysis flash. This finding suggests that the intermediate state is not formed by direct photoabsorption from the ground state but involves some intermediate collision processes, which would be consistent, for example, with the suggestion that the lower state is a $^3\Pi_{2u}$.

Considerations of the spin orbit effect leads to the conclusion that the lowest of the manifold $^3\Pi_g$ ionic states is the $^3\Pi_{2g}$. Since in general, we expect that the lowest state will be the most populated state under collision-dominated conditions, the 2g-2u transition is also favored from this point of view. However, this manifold of states, being closely spaced in energy, may also be fully mixed by collisions so that the radiation will be emitted from the transition with the largest transition probability.

However, in Cl_2, where a rotational analysis of the spectra has been possible [BN63], the lower state appears to be conclusively determined as the $B^3\Pi_{0_u^+}$. Unfortunately, in Br_2, the rotational transitions were not resolved and although the vibrational constants fit the $B^3\Pi_{0_u^+}$ state, the lower state identification is not definite. Additional high resolution spectroscopy in I_2 and Br_2, probably conducted with tunable lasers, is clearly needed to resolve these questions.

The lower state identification is clearly important to the understanding of the ultimate performance of the halogen lasers, since it bears on the problem of lower state quenching or removal. The $B^3\Pi_{0_u^+}$ state, for example, is known to be readily predissociated by collisions and the cross sections have been measured [CB73]. The $^3\pi_{2u}$, on the other hand, cannot be predissociated and may require high pressures to avoid bottlenecking. The recent laser demonstrations on Br_2 by Murray, Swingle, and Turner [MST76] suggest that Br_2 collisions may be important in removing the lower laser level.

The Cl_2^* spectra observed in our experiments differ markedly from those observed by Chen and Payne (CP76). They observe a narrow unstructured peak near 2600 Å at low Ar pressures, which changes to a broad continuum as the Ar density is increased to 780 torr. In our case, the observations made at 4-5 atm of Ar show the broad continuum and a narrower structured band at low Cl_2 density (0.15 torr). At high Cl_2 density (3.8 torr), the broad continuum is almost completely quenched and the structured band is prominent.

We also observed the effect of mixtures of several halogens together. If two halogens are present (e.g., Cl_2 and Br_2, Cl_2 and I_2), essentially all the light emission will be from the heavier homonuclear diatomic. Normally, we do not observe emission from mixed diatomics (IBr). This effect has been observed over a relatively wide range of additive pressure ratios.

C. Signal Time Behavior

1. Leading Edge and Lifetime Measurements

One of our goals is to determine the energy transfer mechanisms in the Ar/I_2 system, and its kinetic processes and rate constants. We have measured the time history of the major excited species, namely Ar^*, I^*, and I_2^*, as a function of both Ar and I_2 pressures and have determined several rate constants from these data.

Figure 10 shows a recording of the time behavior of the light emission from the 342 nm band of molecular iodine. Unlike the traces from the atomic iodine emission at 206.2 nm and other wavelengths, a characteristic feature occurs within the first few nanoseconds after the electron beam pulse is initiated. This feature does not appear when HI is the additive gas. We have concluded that this peak arises from iodine molecules directly excited by the electrons. This initial fast peak is superimposed on the rising portion of the main feature that reaches a peak intensity many tens of nanoseconds later. The rise time and peak intensity of the main (slower) emission are strongly dependent on iodine density. As the vapor pressure increases above 0.25 torr (room temperature) the leading edge feature gradually becomes completely dominated by the second peak, making quantitative representations of the faster peak more difficult. These data were therefore taken with iodine vapor pressures below 0.25 torr and with argon pressures below 2.5 atm.

The characteristic decay time of the feature is acquired as follows: The Tektronix 7912 transient digitizer is used to average the output from five successive excitations. The iodine is maintained in the cell during the five shots; no flushing or other procedures on the medium are made between shots. Approximately once or twice a day the cell is heated above $50^{\circ}C$ and pumped out to reduce the contribution of volatile impurities.

Figure 11 shows typical data from such an averaging procedure. In this example, to enhance the resolution over the time of the initial peak,

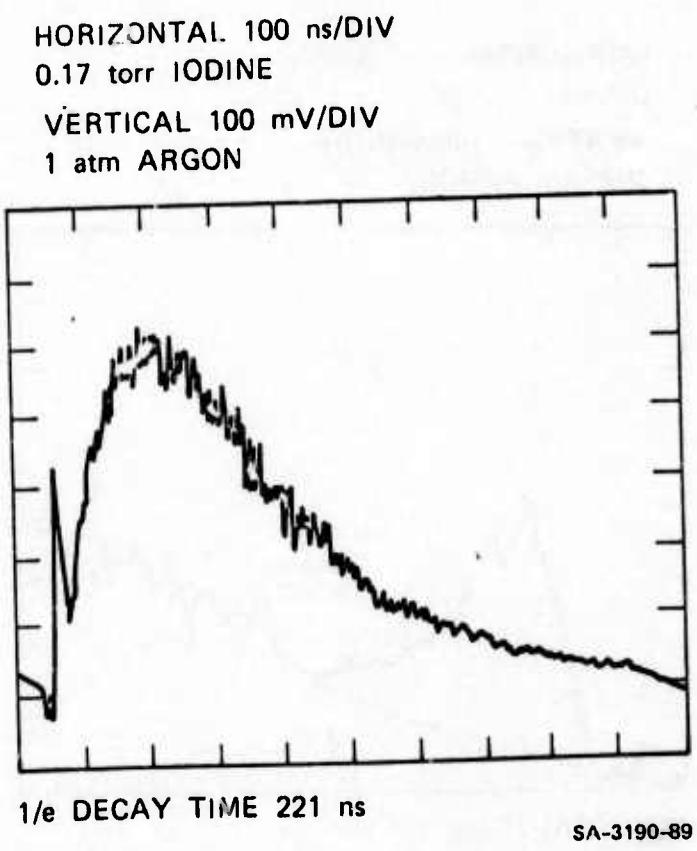

Figure 10. I_2 emission at 342.5 nm vs time. Horizontal scale 100 nsec/div. Note fast peak is due to direct electron excitation of I_2.

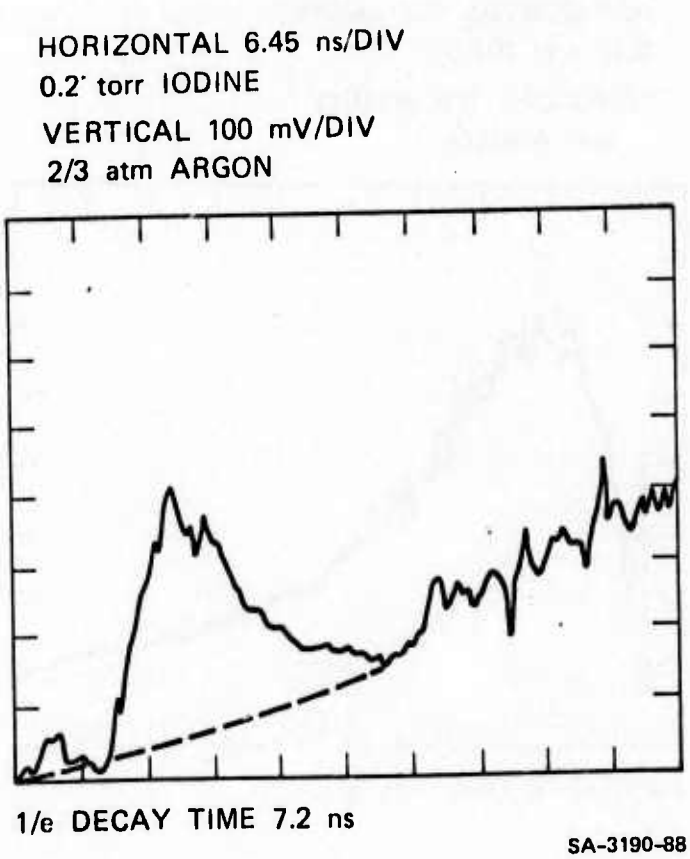

Figure 11. Details of fast peak of I_2 emission at 342.5 nm. Horizontal scale 6.45 nsec/div. Dashed line represents slowly rising emission due to transfer from excited Ar.

we used a 20 nsec/division time scale in the digitizer input. The trace over the peak is then expanded to 6.45 nsec/div under computer control to allow convenient handling of the decay time. We must subtract the signal because of the more slowly rising "main" signal. This contribution is determined by drawing a line through the midpoint of the main peak and extending this line below the initial peak back through the origin. The firing of the Febetron can be determined by observing an impulse on the phototube because of x-rays produced by the electron beam. The passage of the uv light signal is delayed by its time of flight through the spectrometer. The true initial time is near the sharply rising edge of the "fast" signal.

The data taken at 342 nm are displayed in Figure 12 against argon pressure in atmospheres. Above about 0.1 atm a decay time of approximately 6.5 to 7 nsec is shown; and within the scatter of the data, a general independence with pressure is indicated. This pressure independence is necessary if the decay time is to be interpreted as a radiative decay time. The arrow in the figure at 6.7 nsec (~ 150 MHz) indicates the value reported by Sauer et al. [SMC75], who have also analyzed this emission feature.

Below about 0.1 atm of argon, the decay frequency drops sharply with decreasing pressure. This behavior is consistent with a model (also discussed by Sauer) in which the fast peak emission is caused by a multiple step "direct" excitation of the I_2^* state at 343 nm, rather than a collisional excitation transfer from Ar^* or I^*. The fast electrons (or secondary electrons) produce excited iodine molecules in a variety of excited states most of which do <u>not</u> radiate in the observed band. Subsequent collisions with the argon gas induce electronic and vibrational relaxation down to the potential curve, which can radiate at 343 nm.

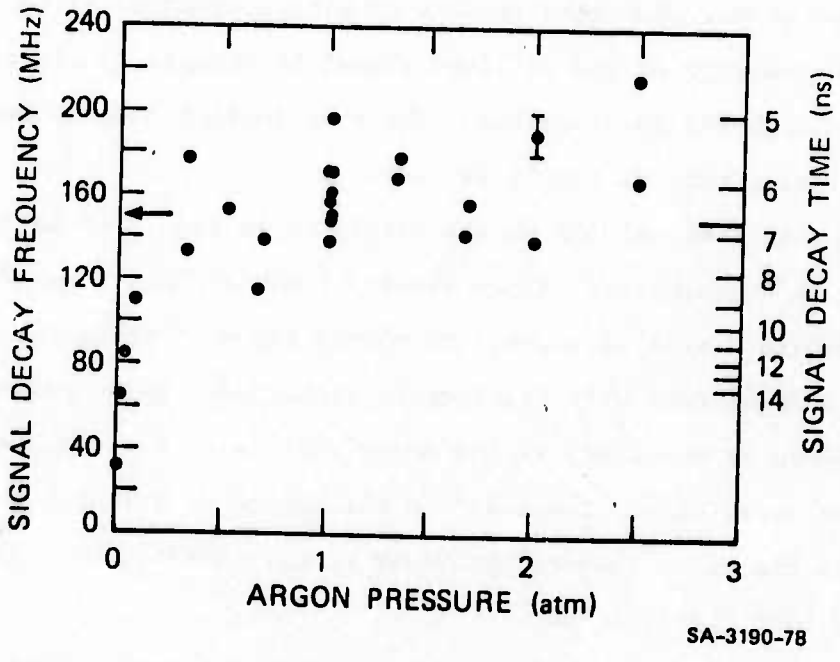

Figure 12. Exponential decay rate for the inital fast I_2 emission peak vs Ar pressure. Arrow represents radiative rate reported by Argonne group [SM76].

As the argon pressure is reduced to the point where the relaxation processes are slow compared with the radiation time, the apparent decay time will be increased. A crude straight line fit to the data below gives a total relaxation rate constant for the reaction

$$I_2^*(N_1,\nu_1) + M \xrightarrow{k_r} I_2^*(N_2,\nu_2) + M \qquad (9b)$$

where M refers to any collision partner, such as e^- or Ar, and where $I_2^*(N_2,\nu_2)$ refers to the state capable of radiation. The rate constant k_r is approximately $7 \pm 3 \times 10^{-11}$ cm^3/sec, assuming the collision partner is Ar. This is consistent with and within the value determined by Sauer by an alternative analysis of the wavelength variation of the decay.

2. Decay Frequency of Molecular and Atomic Emissions

For the dominant emission in the 343 nm band of molecular iodine, a semilog plot of the signal intensity as a function of time after the Febetron pulse shows a straight line behavior over more than two orders of magnitude in intensity (see Fig. 13). This linear behavior holds over a wide variety of iodine and argon pressures. In our experiments, the iodine pressure was varied between 0 to 2 torr, the argon pressure, from 0 to 10 atm. Data taken with other iodine bearing additives, such as CF_3I, CH_3I, and HI, showed similar behavior over this limited pressure range, as did data from the appropriate bands of bromine and chlorine.

Because of the upper state lifetime of 7 nsec, this straight line behavior will be dominated by a two-body collision involving neutral species in the source terms of the upper states. Such behavior would not hold for the mutual neutralization of two charged positive and negative ion species, for example. We suggest that this source term of the 343 nm band caused the collision

$$I^* + I_2 \xrightarrow{k} (I_2^*)' + I \qquad (9a)$$

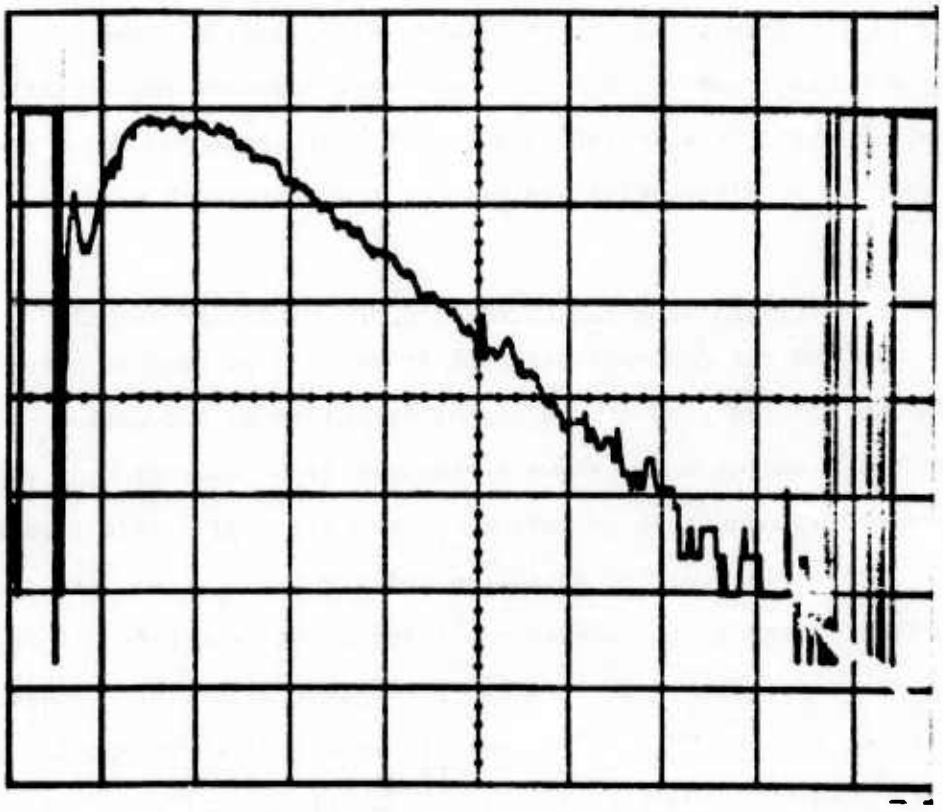

Figure 13. Semilog plot of I_2 emission. Vertical = ℓn Intensity. Horizontal scale 100 nsec/div. Shows a single exponential decay of nearly five powers of e.

followed by rapid electronic and vibrational relaxation to the level capable of radiating in the 343 nm band.

$$(I_2^*)' + M \rightarrow I_2^* + M \ , \qquad (9b)$$

where M is an appropriate collision partner, for example, a rare gas atom.

The decay frequency determined for the 343 nm emission when plotted vs. I_2 density yields a rate constant for Reaction (9a) above of $1.3 \pm .2 \times 10^{-9}$ cm^3/sec (see Fig. 14), which is found by measurements with iodine vapor pressures between 0.01 and 2.2 torr and argon pressures between 0.5 and 5 atm. Most of the data were taken at 342.5 nm, the wavelength of maximum intensity, but we also made several checks at wavelengths down to 325 nm and did not observe significant departures from this value.

Most of the decay time data reported here were taken at 342.5 nm with a resolution of approximately 0.3 nm. To check the wavelength dependence on this emission, we occasionally checked the emission at 330.0 nm but did not observe a strong difference from that at 342.5 nm. Using room temperature iodine (0.25 torr), we also made a more detailed scan by taking data every 0.2 nm between 336.3 and 338.5 nm. This 2.2 nm scan includes a "peak" and a "valley" in the emission of the bluer extremes of the 343 band. Again, we observed no systematic variation in the decay time within the scan (to within approximately ±1 nsec) nor any difference between the decay time in this range and that at 342 nm within the limits of the scatter of our data.

We held the iodine vapor pressures fixed (normally at the room temperature value of ~ 0.25 torr) and varied the argon pressure between 0 and 10 atm. Figure 15 displays these decay frequency data. While appreciable point-to-point scatter in the data is observed, a straight line drawn through the points has a slope that yields a rate constant value of 2.3×10^{-14} cm^3/sec. This figure sets an approximate upper limit on the quenching of the I_2^* precursor by atomic argon. For example, $I^*(^4P_{5/2}) + Ar \rightarrow I(^2P_{3/2}) + Ar + h\nu$.

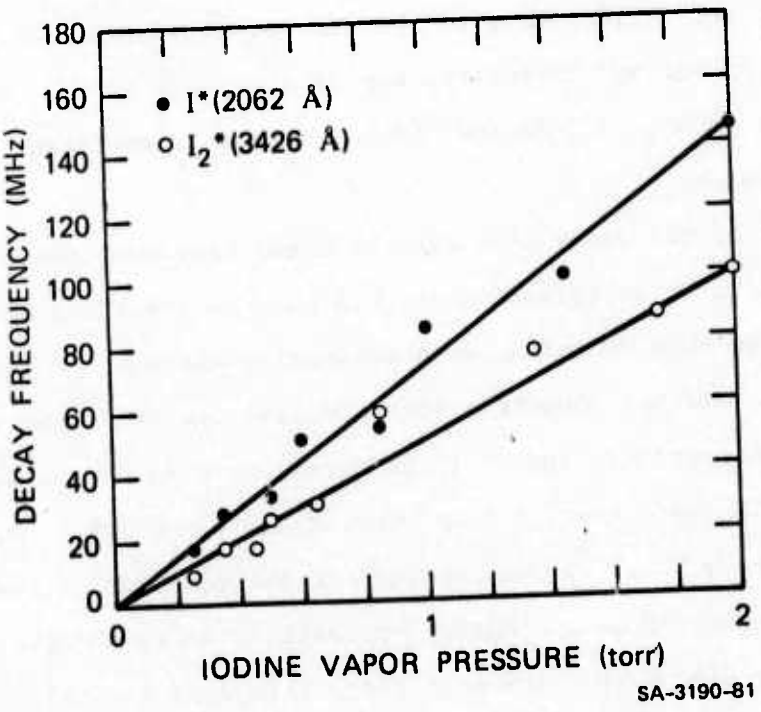

Figure 14. Decay frequency for I_2 (342.6 nm) and I (201.2 nm) emissions vs I_2 vapor pressure with Ar pressure constant.

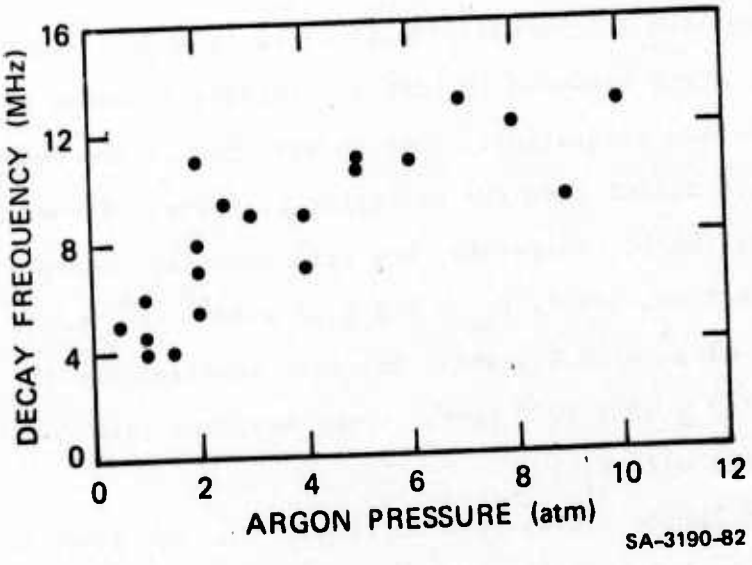

Figure 15. Decay frequency for I_2 (342.5 nm) emission as a function of Ar pressures with I_2 vapor pressure constant (0.25 torr).

We have monitored several of the excited I atom levels (see Figure 4) by observing their emission lines at 206.2, 161.9, 178.3 and 183.0 nm. The first three of these have the same decay rates, which are slightly faster than the I_2^* (342.5 nm) decay rates. A plot of the brightest atomic line, 206.2 nm, and the I_2^* decay rates vs. I_2 vapor pressure is given in Figure 14. The $I^*(^4P_{5/2})$, 183.0 nm, which is the lowest of the excited electronic states, has the same decay rate as the I_2^* emission, indicating that it is the dominant precursor or source term for I_2^*.

We expect the I atom emission lines to be radiatively trapped by ground state atoms produced by both the initial transfer reaction (8c) and by the e-beam excitation. This is verified by the decay rates which are much slower than the radiative lifetimes of some of the atomic levels [L67]. Therefore, the rate constant observed for the $I(^2P_{3/2})$, 206.2 nm, level, $k_{9a} = 1.5 \pm .2 \times 10^{-9}$ cm^3/sec is measuring the reaction of I^* with I_2, while the rate constant for the $^4P_{5/2}$ level $k_{9a} = 1.3 \pm .2 \times 10^{-9}$ measures the reaction rate for the major I^* atom species with I_2.

Myer and Samson [MS70] have noted that for the lines with wavelengths shorter than 183.0 nm, direct absorption by I_2 to highly excited levels becomes important; that is, these lines have photoabsorption cross sections of approximately 3×10^{-17} cm^2. With our cells, the absorption path length is 12.5 cm. Thus, the density for an e fold absorption is $2.7 \cdot 10^{15}$ cm^{-3} or approximately 0.1 torr. Mulliken [M71] has reviewed the excited molecular iodine products that arise from absorptions in this wavelength region; absorption by other additives (CH_3I) is less well understood.

The relative time dependent density of the Ar^* population can be monitored by adding a small amount of N_2 gas to the mixture. Since the N_2(C-B) second positive series at 337, 358 nm, etc., can be produced only by collisions with Ar^* atoms and not by Ar_2^* [HGH74]. The time behavior of the emission at 358 nm will follow the density of Ar^* within the limitations of the 40 ns lifetime of N_2(C), as well as its quenching by argon.

With the addition of 0.02 torr of N_2, we observe a signal that initially appears to decay exponentially, but that, at late times, decays much more slowly than would be predicted by the exponential behavior. We consider only the early part of the decay and compute the decay frequency. These values are compared with the decay frequencies at 206 nm nm I^* and 342 nm I_2^* vs. argon pressure in Figure 16. There is a pronounced difference in the curves; the iodine emission appears not to follow the Ar^* decay. Of course, at higher argon pressures, a significant loss of Ar^* population is in the formation of Ar_2^*:

$$Ar^* + 2Ar \rightarrow Ar_2^* + Ar$$

which has a rate constant of 10^{-32} cm^6/sec [HGH74]. However, collisions with electrons that have energies greater than 1 eV will establish an equilibrium between Ar^* and Ar_2^* [L76]. Thus, Ar^* could follow Ar_2^*, which is lost by radiation ($\nu_{max} \cong 40$ MHz) and by collisional quenching by I_2.

3. Signal Rise Time

In general, the rising portion of the I_2 signal cannot be represented by a single exponential beginning with the Febetron shot.

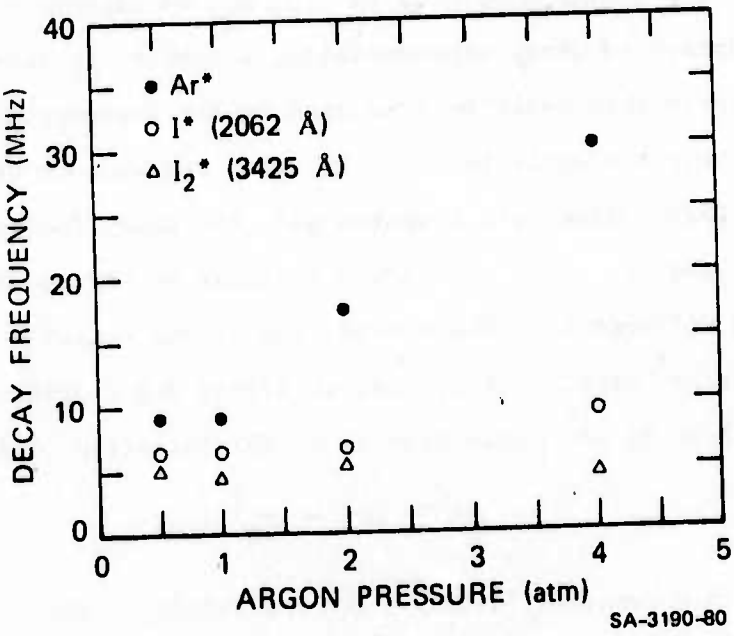

Figure 16. Decay frequency of I_2 (342.5 nm) and I atom (206.2 nm) emissions and Ar^* density (monitored by Nitrogen 2nd positive 357.9 nm emission) vs Ar pressure with I_2 vapor pressure constant.

However, we have not yet attempted to precisely characterize the temporal behavior of this signal. We have recorded, instead, the total time (0 → 100%) the signal takes to reach peak height. This time varies considerably with variations in the argon pressure or the iodine vapor pressure. Also, we observe a considerably faster rise time for the I_2^* signal produced in iodine bearing compounds, such as CF_3I or HI. These data are shown in Figure 17a.

A significant variation observed in the signal rise time for different species is reduced at the highest iodine vapor pressures studied. Figure 17b shows observations of the rise time of Ar^* (determined by observing $N_2(C)$ emissions from trace additives of N_2), I^* (at 206.2 nm), and I_2^*. The Ar^* rises most rapidly. This variation in rise time is plausible within the context of our kinetic model, since we believe that Ar^* is the collisional precursor of I^*. However, these data should not be quantitatively interpreted. In recording the full rise time, we include in the data a considerable contribution of the (possibly) exponential loss term in the emission. Among the several possible loss terms for the Ar^* are Ar_2^* production and quenching of Ar^* by I_2.

At the higher iodine pressures, the rise time of the I^* emission follows more closely the Ar^* rise. The peak time of the molecular iodine emission at 343 nm, shown for comparison, lags behind its plausible precursor, atomic iodine at all iodine pressures.

4. Molecular Argon Emissions and Quenching

We attempted to directly observe the quenching of the Ar_2^* population by measuring the decay frequency as a function of iodine pressure. To lower the iodine vapor pressure sufficiently, we cooled the cell by pumping a slurry of dry ice and methanol through copper coils wound around the cell. However, because of the strong absorption of the 126.0 nm Ar_2^* excimer emission, the iodine vapor pressure range

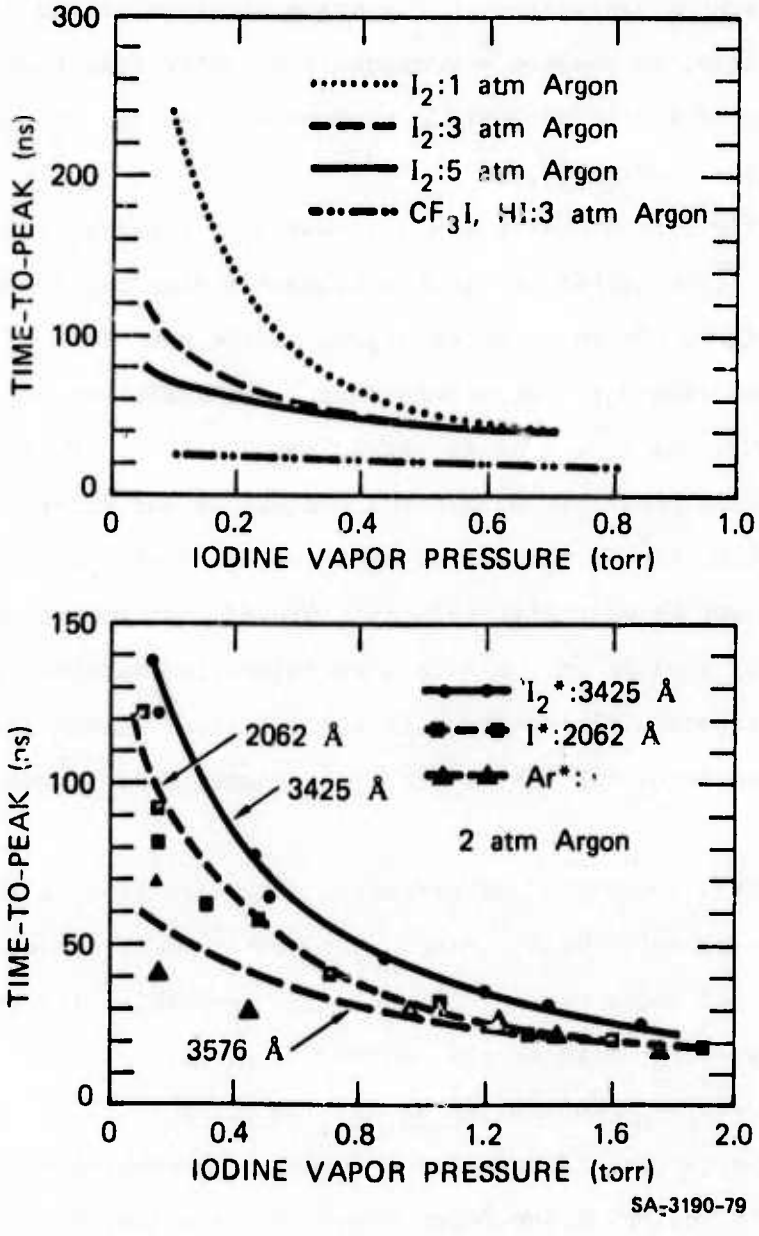

Figure 17. Time to peak (from e-beam pulse to peak emission): a) for I_2 emission (342.5 nm) at various Ar pressures and with I_2, CF_3I, and HI as the I atom source; b) for I_2^*, I^* and Ar^* (monitored by N_2 2nd positive).

over which we could observe a signal was too small to observe the effect of quenching. Under these conditions (3 atm Ar, 0.005 to 0.01 torr I_2), we observed that the argon emission has a rise time (time-to-peak) of $\simeq$ 60 ns and a decay time (1/e) of 130 ns; the time-to-peak of the iodine signal was $\simeq$ 120 ns with a decay time of 1-2 μs. Above $\simeq$ 0.07 torr, the 1260 Å band could not be observed because of absorption.

5. Signal Peak Intensity

The peak intensity of the emission signal can be related to the net gain of a potential laser system. In determining this gain, we have found it particularly useful to make direct comparisons with the second positive emission at 337.1 nm from mixtures of argon and nitrogen.

Precise measurements of the signal peak intensity in our system have been occasionally subject to uncertainty, particularly at elevated iodine vapor pressures. First, at high iodine pressures and higher argon pressures, where the signal rises and falls rapidly, the exact value of the peak can be significantly shifted by noise, etc. Also, absorption by iodine condensed on windows can cause reduction of the signal. Finally, the outgassing from the walls of volatile impurities may absorb the emitted radiation and attenuate the signal.

For the 343 nm molecular iodine signal, the data up to 1 torr iodine pressure are reasonably linear (within the scatter) in iodine pressure. As the pressure rises above 1 torr, the slope of this curve gradually decreases. We have observed a leveling off above 2 torr, and a decline in the signal value, but we do not yet have sufficient data to eliminate the above mentioned absorptions as being the source of this effect.

The atomic iodine emissions reach a peak intensity when the iodine vapor pressure is in the vicinity of 0.25 torr. We have traced the sharp decrease in the 206 nm signal above that value; we have been unable to observe the 183 nm signal above 0.25 torr because of the small signal values.

The molecular iodine signal generated from HI and CF_3I is significantly larger in peak intensity than that from molecular iodine below an additive pressure of 2 torr (Figure 18). Above 2 torr, where we have uncertain data on I_2, we observe a broad general signal decrease with the half point (i.e., signal value, half of the peak height) found near 20-40 torr of additive.

6. Integrated Intensity

The integrated intensity of the signal is a measurement of the total light emitted in the band at all wavelengths. Measurements of this value can be used to estimate the potential efficiency of a laser medium (see Section IV). Our spectroscopic measurements provide the information necessary to make the appropriate integrations over wavelength. Most of our data are taken with spectrometer slits set to provide ~ 0.33 nm resolution. Integration over time has been provided, most recently, by direct numerical integration of the digitized signal; however, most of our data are in the form of oscilloscope photographs from which the integrations were performed "by hand", and our integrated intensity data show considerable scatter. For clarity, we present here data at 1, 3, and 5 atm pressure for iodine pressures between 0 and 2 torr. These data were generated by plotting peak height (V_o) time-to-peak height (τ_o) and decay time τ_e (1/e folding time). From curves drawn through the data points, we can determine an approximate value for the time-integrated intensity by using the formula for the area within a triangle $A = V_o(\tau_o+2\tau_e)/2$.

While this method is clearly limited, it does indicate trends in the data and is easy to implement. Data determined by this method are shown in Figure 19. At all argon pressures, there is a maximum in the relative integrated intensity for iodine vapor pressures between 0.5 and 0.8 torr.

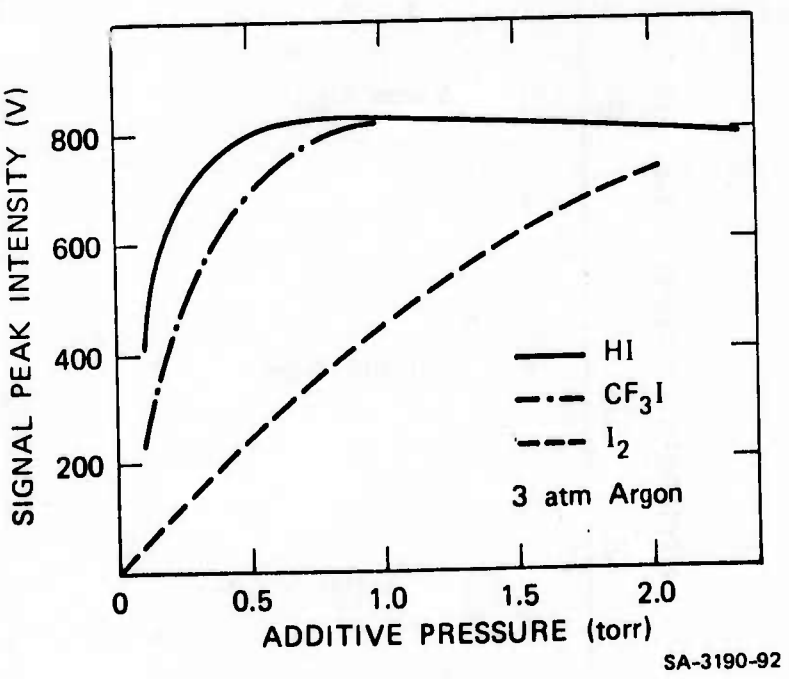

Figure 18. Peak intensity for I_2^* emission (342.5 nm) as a function of the partial pressure of the I atom source in 3 atmospheres of Ar.

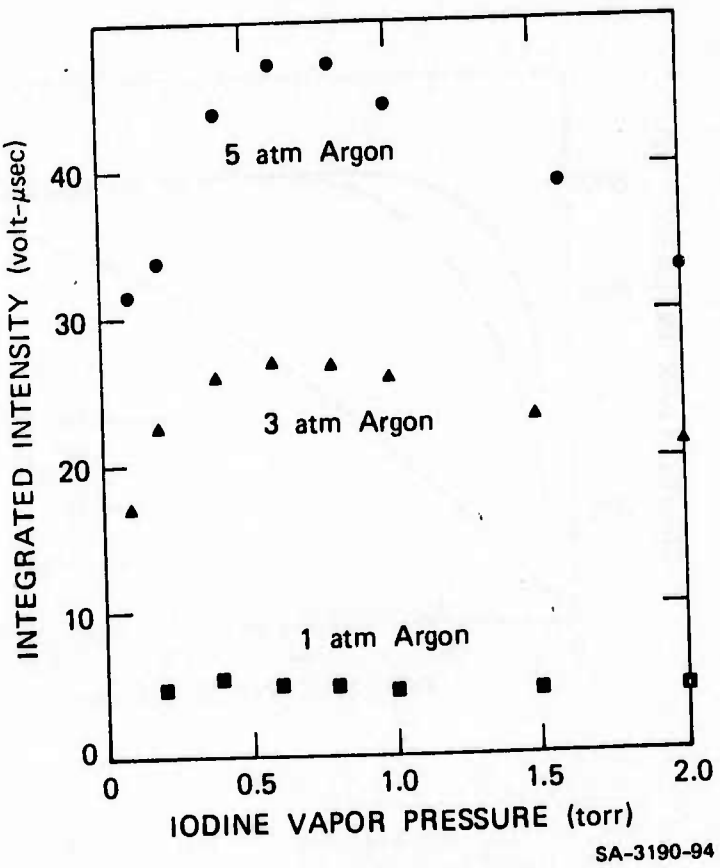

Figure 19. Integrated intensity for I_2 (342.5 nm) emissions vs I_2 vapor pressure at 1, 3 and 5 atmospheres of Ar. The integrated intensity is a measure of the total number of fluorescent photons in the I_2 emission band.

If the iodine vapor pressure is held fixed at room temperature, a linear relationship can be observed between argon pressure and integrated intensity. The data in Figure 20, which show this effect, were taken the same day and were directly integrated by numerical methods. We have not yet systematically studied this behavior at elevated iodine pressures (the data in Figure 20 indicate a possible systematic deviation from linearity in the 1 atm values above 0.25 torr).

The fluorescence yield is defined to be the ratio of the number of excited argon atoms and excimers produced. The calibration of the excitation source and detection efficiency is accomplished by comparison with the fluorescence of a 5% Ar/N_2 mixture and model calculations [HGH74,MHH75]. We calculated the Ar/N_2 fluorescence yield to be 8.8% at 2 atmospheres, and that the pressure dependence was

$$FY(Ar/N_2) = 17.6\%/[Ar]_{atm}$$

The model predicts a pressure independent integrated fluorescence; experimentally we find a pressure independent value.

The fluorescence yield of Ar/I_2 is then computed from

$$FY(Ar/I_2) = FY(Ar/N_2) \frac{IF(Ar/I_2)}{IF(Ar/N_2)}$$

$$= 64 \pm 20\% \text{ at 3 atom and 1 torr } I_2 .$$

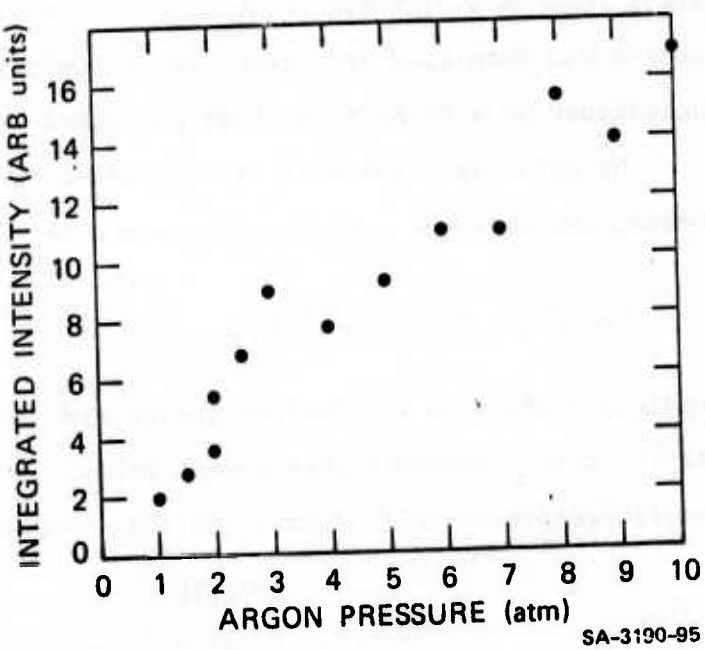

Figure 20. Integrated intensity for I_2 (342.5 nm) emission vs pressure of Ar at a constant I_2 vapor pressure of .25 torr (see caption to Figure 19).

IV STATUS OF Ar/RI KINETIC MODEL AND LASER IMPLICATIONS

As suggested in Section I, the development of efficient high energy lasers will depend on a sufficiently detailed characterization of a variety of collisional and radiative processes. In this section, we discuss the status of the determination of the rates and cross sections for these critical processes relevant to Ar-I_2 mixtures, with particular emphasis on their relevance to laser development. The relevant rate constants and cross sections are collected in Table IV. An example of a discharge pumped Ar/I_2 laser is calculated.

A. Energy Flow Pathways

In Section II we proposed that I_2^* (343 nm) emission results from the neutral energy transfer chain

$$Ar^* \rightarrow I^* \rightarrow I_2^* \quad .$$

As described in Section III, we have followed the temporal and pressure behavior of these species through the Ar_2^* (126 nm), Ar^* [N_2(357 nm)], I^* (183 nm, 206 nm), and I_2^* (343 nm) fluorescence decays. While this simple kinetic model is consistent with all our experimental observations, we cannot exclude some alternative schemes that may be important under different excitation conditions.

(i) Production of I_2^*--The observation that the I_2^* emissions can persist over a time scale longer than the excitation pulse or the decay of the energy stored in the argon excited states (see Section III), combined with the short I_2^* radiative lifetime, requires the existence of a reasonably long-lived energy transfer intermediate. This excludes direct excitation transfer

$$Ar_2^* + I_2 \rightarrow I_2^*$$

as the dominant excitation pathway. Furthermore, direct excitation transfer is obviously inapplicable in the Ar/HI and Ar/CF_3I systems.

Through radiation trapping, I^* becomes an acceptable storage intermediate. However, excitation storage is also possible in an ionic reaction scheme. Indeed, the early observations of efficient fluorescence and laser action from the ionic-to-covalent 343 nm transition in I_2 led many researchers to speculate that an ion-ion recombination mechanism was a likely path [EB75b]. Consider, for example,

$$I^+ + I^- + Ar \rightarrow I_2^* + Ar \quad . \tag{12}$$

Considerable evidence now indicates that the ion recombination does not contribute in a major way to the I_2^* formation under our excitation conditions. The production of I^- would be controlled by competition for free electrons between the two reactions

$$e + Ar_2^+ \rightarrow Ar^* + Ar \tag{2}$$

$$e + I_2 \rightarrow I^- + I \quad . \tag{13}$$

The rate constant for Reaction (2) varies from 10^{-7} cm^3/sec at 1 eV to 10^{-6} cm^3/sec [BB70] at thermal energies. The rate constant for Reaction (13) is 1.8×10^{-10} cm^3/sec [T69] at thermal energies and increases to 2.8×10^{-10} cm^3/sec at 0.27 eV electron energy and also increases with higher gas temperature. In Ar at pressures above 1 atm, the Febetron produces electron densities $n_e \geq 10^{15}/cm^3$, giving a rate for (2) of $\geq 10^8$/sec. The attachment rate at 1 torr I_2 is $\leq (4 \times 10^{-10} \times 3 \times 10^{16} \cong 10^7$/sec). The electrons then recombine with Ar_2^+ to yield Ar^* far more rapidly than they attach to I_2 to yield I^-. Thus, the kinetic rates support the conclusion that I_2^* is produced mainly by way of neutral reactions. Of course, under lower excitation density conditions where the electron density is low and electron-ion recombination slowed, electron attachment will become more important.

The observed I_2^* decay and its pressure dependence provides evidence for an I^* intermediate. At each I_2 pressure, the I_2^* and I^* emissions showed purely exponential decays for at least two decades. If the ion-ion recombination processes were dominant, then the decay rate would be proportional to t^{-1} and clearly, nonexponential. In addition, each of the decays showed a linear dependence on the I_2(RI) pressure (and very little dependence on argon pressure) as would be expected from the reactions

$$I^* + I_2 \rightarrow I_2^* + I \qquad \text{or} \qquad (9a)$$

$$I^* + RI \rightarrow I_2^* + R \qquad . \qquad (9c)$$

An ion-ion recombination reaction, such as (12), would be expected to have a much more complicated pressure dependence.

Concerning the rates for ion-ion recombination at high pressures, Brau and Ewing [BE75r] and others [HTH75] suggest that three-body Thompson ion-ion recombination (Reaction 12) should be exceedingly fast at high pressures. They suggest a rate coefficient of 2×10^{-25} cm^6/sec. However, experimental determinations [JKB65] of the ion-ion recombination rates in oxygen and air indicate that the three-body enhancement saturates in the region of 1-2 atm at an effective two-body rate coefficient of $1\text{-}2 \times 10^{-6}$ cm^3/sec. At higher pressures, the recombination is further slowed by the reduction of ion mobility [B75].

(ii) Production of I^*--These arguments lead us to conclude that the last step of the energy transfer chain is a reaction of an excited iodine atom, as in Reactions (9a) and (9c). Finding the major reactions that produce I^* then becomes important. The most plausible candidate schemes appear to be:

$$\left.\begin{matrix} Ar^* \\ Ar_2^* \end{matrix}\right\} + RI \rightarrow ArI^* + R \rightarrow Ar + I^* + R \qquad (8a,b,c)$$

$$Ar_2^* \rightarrow 2Ar + h\nu \ (126 \text{ nm}) \qquad (7)$$

$$h\nu \ (126 \text{ nm}) + RI \rightarrow R + I^* \qquad (14)$$

$$\left.\begin{matrix} Ar^* \\ Ar_2^* \\ h\nu \ (126 \text{ nm}) \end{matrix}\right\} + RI \rightarrow RI^+ \qquad (15a,b,c)$$

$$RI^+ + e \rightarrow R + I^* \quad . \qquad (16)$$

Experimentally, these competing pathways are rather difficult to distinguish. The suggestion of an ArI^* intermediate that immediately predissociates is consistent with observations of Setser et al. [GSC76], who observed only atom production in both I_2 and Br_2 interactions with Ar^*. The three alternative paths by which the energy is transferred from the argon (Reactions 8a,b and 14) will produce essentially the same temporal behavior. The argon atoms and excimers are coupled through the low energy electrons [L76], and the 126 nm intensity is proportional to the excimer and atom populations.

At RI pressures above 1 torr, radiative transfer (14) is not expected to be important. The observations of N_2 (357 nm) as a monitor of Ar^* (see Section III) illustrated that Ar^* reacts rapidly with I_2. Few of the argon excimers will have time to radiate. For example, at 1 torr of I_2, the transfer rate is 5×10^7/sec, and the Ar_2^* radiative rate is $< 4 \times 10^7$/sec for any Ar density. At low I_2 or RI pressure ($\leq$ 0.1 torr), much of the stored energy could appear as 126 nm radiation. Even at these low I_2 pressures, the enormous photoabsorption cross section (10^{-16} cm^2 [MS70]) of I_2 should absorb the excimer radiation and could lead to significant I^* and hence I_2^* emission.

Choosing between energy transfer from Ar^* or Ar_2^* is more difficult. If energy transfer from Ar^* were the dominant channel, the fluorescence yield could be expected to be highest at a low argon pressure, where a larger fraction of the energy is stored in Ar^* than in Ar_2^*. This hypothesis contradicts the observed argon pressure dependence, Figure 2, and suggests that transfer from Ar_2^* may be more important.

We have no direct evidence with which to assess the relative importance of the ionization-recombination, Reaction (16) pathway, as a source of I^* as opposed to dissociative energy transfer (8). Under our excitation conditions, this recombination would be sufficiently rapid to be kinetically indistinguishable from an energy transfer reaction. Nevertheless, we may argue in favor of a completely neutral reaction scheme.

Assuming that transfer from Ar_2^* may be the most effective, we note that such transfer is the least likely to yield I_2^+ by Reaction (16). The argon excimer has enough energy to ionize I_2 (10 eV vs 9.3 eV), but the reaction mechanism should be dominated by the charge transfer channel ($Ar_2^+ + I_2^-$). This channel should couple only weakly with ionization (it requires a two-electron interaction) and should selectively lead to the ion-pair product Ar^+I^-, which would predissociate to I^*. Energy transfer from Ar^* to I_2 is more likely to lead to ionization because of its higher excess energy, although neutral products could still be favored. There is evidence that photoabsorption of 126 nm radiation by I_2 may yield exclusively ionic products (mostly $I_2^+ + e$) [MHI60].

Further, the close similarity between the observations in I_2, HI, CF_3I, Br_2, HBr, and Cl_2 suggests a common energy flow scheme. If photo or energy transfer ionization and subsequent recombination were dominant, we might expect greater differences caused by the different ionization potentials and presumably different recombination channels.

B. Radiation and Quenching

The reaction

$$I^* + RI \rightarrow I_2^* + R \qquad (9c)$$

will produce in a variety of excited states. The relaxation by argon described in Section III indicates that the excited state population is rapidly collected in the few lowest levels. The high quantum yield indicates that quenching is unimportant at I_2 pressures $\sim$ 1 torr. The short radiative lifetime (7 nsec) results in a high stimulated emission cross section (10^{-15} cm^2).

The short radiative lifetime complicates a kinetic measurement of the quenching reactions since the time decay follows the slowest reaction step (I^* + RI). The RI pressure dependence of the fluorescence yield can be used to monitor the relative importance of radiation and quenching. By such a technique we find that quenching by HI (Reaction 11b) proceeds with a rate coefficient of $4 \pm 2 \times 10^{-10}$ cm^3/sec. Such a determination is complicated in CF_3I by absorption of the I_2^* (343 nm) radiation and in I_2 by the presence of impurities. We conclude in both of these cases that the rate coefficient should be less than 10^{-9} cm^3/sec (Reactions 11a and 11c).

Removing the lower laser level could conceivably prove difficult since it is a bound electronic state. This problem must be further assessed to assign the lower state and determine its relaxation rate. Nevertheless, relaxation in the high vibrational levels should be rapid (for example, 2×10^{-11} cm^3/sec for the B state [CB73]).

C. Efficiency, Extraction, and Stability

The two energy transfer steps we have discussed produce the I_2^* radiating species on a rather long time scale. The instantaneous population of I_2^* is rather low due to its short radiative lifetime and

quenching by the iodine source (I_2, HI, CF_3I). Nevertheless, the high stimulated emission cross section will lead to significant gain. We have seen that, under appropriate conditions, the upper laser level is populated with remarkable selectivity. To illustrate that this selectivity can be converted to efficient laser operation, we consider an example laser system.

We suppose that the laser pump consists of an electron-beam controlled discharge in which the electron beam contributes the ionization and a sustaining electric field provides most of the excitation energy.

(a) Primary electrons + Ar → Ar^+ pump rate = 5×10^{21} cm/sec

(b) Secondary electrons + Ar → Ar^* pump rate = 1.5×10^{22} cm/sec

These relatively modest excitation rates appear typical of the electron-beam controlled discharges under development. We suppose that the pump time is long compared with the various kinetic processes. The ion density is controlled through the competition between ionization and recombination.

$$(Ar_2^+, I_2^+) + (e, I^-) \rightarrow \text{neutrals} \qquad k_2 \sim 10^{-6} \text{ cm}^3/\text{sec} \quad . \quad (2)$$

This yields an ion density of $N_t = 7 \times 10^{13}$ cm^{-3}.

Let us choose a gas composition of 3 atm Ar, 1 torr I_2. The electron attachment to I_2 competes with electron and ion-ion recombination through

$$e + I_2 \rightarrow I^- + I \qquad k_{13} \sim 4 \times 10^{-10} \quad . \quad (13)$$

The quasi-steady state concentrations are calculated through

$$\frac{d}{dt}[I^-] = k_{13}[I_2][n_e] - k_{12}[I^-][N_t] \quad .$$

By charge balance $N_t = n_e + I^-$. So,

$$n_e = \frac{k_{12}N_t^2}{k_{13}I_2 + k_{12}N_t}$$

or under the assumed conditions

$$n_e = 6.1 \times 10^{13} \text{ cm}^{-3}$$

$$I^- = 9 \times 10^{12} \text{ cm}^{-3} \quad .$$

Under these conditions, we find that Ar_2^+ should be the dominant positive ion. Electron recombination should then yield mostly Ar^*, so that the net production rate of Ar^* is the total pump rate of 2×10^{22} cm^3/sec. At three atmospheres, the radiative rate, k_7, for Ar_2^* is only 8×10^6 sec^{-1}, so that nearly every Ar^* or Ar_2^* will find an I_2 to which to transfer its energy. Hence, we have

$$Ar^* = \frac{2\times10^{22}}{8\times10^6 + 1.8\times10^{-9}[I_2]} = 3 \times 10^{14} \text{ cm}^{-3} \quad .$$

Similarly, the I^* density is computed from

$$I^* = \frac{1.8\times10^{-9}[Ar^*][I_2]}{1.3\times10^{-9}[I_2]} = 4 \times 10^{14} \text{ cm}^{-3} \quad .$$

Finally, the I_2^* density is set by its radiation and quenching

$$I_2^* = \frac{1.3\times10^{-9}[I^*][I_2]}{1.4\times10^8 + 10^{-9}[I_2]} = 1 \times 10^{14} \quad .$$

With a stimulated emission cross section of 1.3×10^{-15} cm^2, this yields a small signal gain, assuming fast removal of lower states, of

$$G = 1.3 \times 10^{-15}[I_2^*] = .13 \text{ cm}^{-1} .$$

The competing absorptions are photoionization of I^* and photodetachment of I^-. Using a cross section of 2×10^{-17} cm^2 for both of these [R69], we find them to be negligible as a source of absorption. However, the photon flux limitations referred to in Section I suggest that we must avoid photoionization of I^* since its density greatly exceeds the electron density and its sudden photoionization can lead to inefficiency and instability. We note that if I^* is the lowest excited state ($^4P_{5/2}$), then a 342.5 nm photon has insufficient energy to photoionize and only higher states of I^* could contribute to this problem.

We can make an estimate of the efficiency by comparing the various loss rates given above with the total I_2 fluorescence. Starting from Ar^* we have

$$Ar^* \begin{cases} \xrightarrow{k_8} I_2^* = 1.8 \times 10^{-9}[I_2] = 6 \times 10^7 \\ \xrightarrow{k_7} Ar_2^* \rightarrow h\nu = 8 \times 10^6 \end{cases}$$

or

$$\frac{6}{6 + 0.8} = 88\% \text{ goes to } I^* .$$

Since the loss of each I^* results in the production of I_2^*, we find the branching ratio for each Ar^* to produce I_2^* is R = .88. Finally, the I_2^* may be quenched or it may radiate:

$$I_2^* \begin{cases} \xrightarrow{k_{11}} 2I_2 \text{ (quenching)} = 10^{-9}[I_2] = 3.2 \times 10^7 \\ \xrightarrow{k_{10}} I_2 + h\nu \text{ (radiation)} = 1.4 \times 10^8 \end{cases}$$

or

$$\frac{1.4}{1.4 + .32} = 81\% \text{ of } I^* \text{ radiates as } I_2^*$$

photons. The net fluorescence yield without considering the electrons becomes .81 x .88 = 71%, which is in accord with our previous measurements [MiH75]. In the laser case, if the cavity flux is sufficiently high, the quenching of I_2^* will not compete with the stimulated emission and the efficiency will improve and permit higher densities of I_2 to be used to insure the rapid and efficient energy flow from Ar^*. Unfortunately, because the lower state removal problem is not fully understood, it is not possible to fully evaluate the extraction efficiency question. However, we can express the efficiency as follows

$$\eta = \text{pump efficiency} \times \text{quantum efficiency} \times \text{branching ratio} \times \text{extraction efficiency}$$

$$\eta = \eta_p \times \frac{h\nu}{E_x} \times R \times \eta_x \quad .$$

In the case of e-beam pumping of Ar/I_2 under optimal conditions

$$\eta = 0.5 \times \frac{3.6}{10} \times 0.88 \times \eta_x = 0.16\, \eta_x \quad .$$

In the case of discharge pumping where the Ar metastables are excited directly with an assumed efficiency of 75%

$$\eta = 0.75 \times \frac{3.6}{11.6} \times 0.88 \times \eta_x = 0.20\, \eta_x \quad .$$

In general, η_x for a cw laser is given by

$$\eta_x = \frac{Q_L}{A + Q_u + Q_L} \quad \frac{T}{T + L\Sigma_a} \left(1 - \frac{P_{(th)}}{P}\right)$$

where Q_u and Q_L are, respectively, the upper and lower state quenching rates, A is the transition probability, T is the mirror transmission, L

is the cavity length, Σ_a is the sum of photon absorbers times their absorption cross sections, P is the rate of upper state pumping, and $P_{(th)}$ is the threshold pumping rate. This expression clearly shows the importance of a medium in which $Q_L \gg A + Q_u$ and $L\Sigma_a \ll T$, and the laser should be operated well above threshold. In the case of Ar/I_2, $Q_L \geq 10^9$ sec^{-1} and $P \gg P_{(th)} \simeq 10^3$ watts/cm^3.

D. Summary

An experimental study of the energy transfer kinetics in e-beam pumped argon-halogen mixtures has been carried out with particular emphasis on Ar-I_2 mixtures. For the high excitation density conditions of a fast e-beam pump the kinetics are dominated by a two-step neutral species model involving energy transfer from $Ar^* \rightarrow I^* \rightarrow I_2^*$. The specificity of this reaction for producing the 3425 Å transition is remarkably high and as a result the projected laser efficiency is very high. The relevant rate coefficients and the radiative lifetime of the transition have been measured. The upper and lower states of the transition have not yet been definitely identified and the degree of bottlenecking of the lower level is not known. The latter is the major undetermined quantity preventing a more complete evaluation of laser performance and optimal pump requirements.

The Ar/RI laser medium can clearly be pumped using either e-beam or discharge pumping. The efficiencies should be similar in both cases. It should also be pointed out that because of the coincidence of the 3425 Å transition with a deep minimum in the absorption of UF_6, I_2 may be a good candidate for a neutron generated fission fragment pumped laser [LMR76].

REFERENCES

ABB75 E. R. Ault, R. S. Bradford, Jr., M. L. Bhaumik, Appl. Phys. Lett. 27, 413 (1975).

B75 D. R. Bates, J. Phys. B.: Atom. Molec. Phys. 8, 2722 (1975).

BAB75 R. S. Bradford, Jr., E. R. Ault, and M. L. Bhaumik, Appl. Phys. Lett. 27, 546 (1975).

BB70 J. N. Bardsley and M. A. Biondi in Advances in Atomic and Molecular Physics, Academic Press, New York, 1970, Chap. I

BBA76 M. L. Bhaumik, R. S. Bradford, Jr., and E. R. Ault, Appl. Phys. Lett. 28, 23 (1976).

BE75y C. A. Brau and J. J. Ewing, Appl. Phys. Lett. 27, 435 (1975).

BN63 A. G. Briggs and R.G.W. Norrish, Proc. Roy. Soc. A276, 51 (1963).

CB73 G. A. Copelle and H. P. Broida, J. Chem. Phys. 58, 4212 (1973).

CP75 C. H. Chen and M. G. Payne, Appl. Phys. Lett. 28, 219 (1976).

EB75a J. J. Ewing and C. A. Brau, Appl. Phys. Lett. 27, 350 (1975).

EB75b J. J. Ewing and C. A. Brau, Appl. Phys. Lett. 27, 557 (1975).

GSC76 L. A. Gundel, D. W. Setser, M.A.A. Clyne, J. A. Coxon, and W. Nip, J. Chem. Phys., to be published

GT74 M. F. Golde and B. A. Thrush, Chem. Phys. Lett. 29, 486 (1974).

HEL73 R. M. Hill, E. J. Eckstrom, D. C. Lorents, and H. H. Nakano, Appl. Phys. Lett. 23, 373 (1973).

HGH74 R. M. Hill, R. A. Gutcheck, D. L. Huestis, D. Mukherjee, and D. C. Lorents, "Studies of E-beam Pumped Molecular Lasers," Tech. Report No. 3, Contract N00014-72-C-0478, SRI MP74-39, Stanford Research Institute, 1974.

HGH75 D. L. Huestis, R. A. Gutcheck, R. M. Hill, M. V. McCusker, and D. C. Lorents, "Studies of E-Beam Pumped Molecular Lasers," Tech. Report No. 4, Contract N00014-72-C-0478, SRI MP75-43, Stanford Research Institute, January 1975.

HHT75 A. K. Hays, J. M. Hoffman, and G. C. Tisione, "Molecular Iodine Laser Near 3400 Å," presented at 2nd Summer Colloquium on Electron Transition Lasers, Woods Hole, Mass. 17-19 Sept 1975.

HO76 R. O. Hunter and J. R. Oldrettel, "An assessment of e-beam technologies, etc.", Soc. of Photo-optical Instrumentation Engineers, to be published.

JKB65 H. Jutting, R. Koepp, J. Booz, and H. G. Ebert, Z. Naturforsch, 20A, 213 (1965).

L67 G. M. Lawrence, Astrophys. Jour. 148, 261 (1967).

L76 D. C. Lorents, Physica 82C, 19 (1976).

LEH73 D. C. Lorents, D. J. Eckstrom and D. L. Huestis,"Excimer Formation and Decay Processes in Rare Gases," Final Report MP73-2, Contract N00014-72-C-0457, SRI Project 2018, Stanford Research Institute, Menlo Park, Ca., September 1973.

LMR76 D. C. Lorents, M. V. McCusker, and C. K. Rhodes, "Nuclear Fission Fragment Excitation of Electronic Transition Media," to be published.

LO72 D. C. Lorents and R. E. Olson, "Excimer Formation and Decay Processes in Rare Gases," Semiannual Tech. Report No. 1, Contract N00014-72-C-0457, SRI Project 2018, Stanford Research Institute, Menlo Park, Ca., December 1972.

M71 R. S. Mulliken, J. Chem. Phys. 55, 288 (1971).

MHH75 M. V. McCusker, R. M. Hill, D. L. Huestis, D. C. Lorents, R. A. Gutcheck, and H. H. Nakano, Appl. Plys. Lett. 27, 363 (1975).

MHI60 J. D. Morrison, H. Heirzeler, M. G. Ingraham, and H. E. Stanton, J. Chem. Phys. 33, 821 (1960).

MJ75 J. A. Mangano and J. H. Jacob, Appl. Phys. Lett. 27, 495 (1975).

MP76 J. R. Murray and H. T. Powell, Lawrence Livermore Laboratory Preprint UCRL-78213, May 1976.

MS70 J. A. Meyer and J.A.R. Samson, J. Chem. Phys. 52, 716 (1970).

MST76 J. R. Murray, J. C. Swingle, C. E. Turner, Jr., Appl. Phys. Lett. 28, 530 (1976).

N63 A. N. Nesmeyanov, Vapor Pressure of the Elements (Academic Press, New York, 1963).

R69 D. E. Rothe, Phys. Rev. 177, 93 (1969).

SH75 S. K. Searles and G. A. Hart, Appl. Phys. Lett. 27, 243 (1975).

SMC76 M. C. Sauer, W. A. Mulac, R. Cooper and F. Grieser, J. Chem. Phys., to be published.

T69 F. K. Truby, Phys. Rev. 188, 508 (1969).

THH75 G. C. Tisone, A. K. Hays, J. M. Hoffman, Optics Comm. 15, 188 (1975).

V58 R. D. Verma, Proc. Indian Acad. Sci. A48, 197 (1958).

VS74 J. E. Velasco and D. W. Setser, J. Chem. Phys. 62, 1990 (1975).

WGHR74 C. W. Werner, E. V. George, P. W. Hoff and C. K. Rhodes, Appl. Phys. Lett. 25, 235 (1974).

WTN72 K. Wieland, J. B. Tellinghuisen, and A. Nobs, J. Mol. Spectry. 41, 69 (1972).